Substance P affects exclusively on prototypic neurons in mouse globus pallidus

DOCTORAL DISSERTATION

A thesis submitted in partial fulfillment

of the requirements for the degree of Doctor of Philosophy

By:

Kazuko Mizutani

Supervisor:

Dr. Fumino Fujiyama

Co-Supervisor:

Dr. Fuyuki Karube

Graduated School of Brain Science

Doshisha University

June 2017

Kyoto, Japan

Abstract

Previous studies have suggested that the neurokinin-1 receptor (NK-1R) expressing neurons in the globus pallidus (GP) receive the substance P (SP), presumably released by axon collaterals of striatal direct neurons. However, the effect of the SP on the GP remains unclear. In this study, I identified that the SP-responsive cells comprise of a highly specific cell type in the GP with regard to immunofluorescence, electrophysiology and projection properties. Morphologically, NK-1R-immunoreactive neurons occasionally co-expressed parvalbumin (PV) and/or Lim-homeobox 6 (Lhx6), but not Forkhead box protein P2 (FoxP2), which is mainly expressed by arkypallidal neurons.

Retrograde tracing experiments also showed that some of GP neurons projecting to the subthalamic nucleus (namely prototypic neurons) expressed NK-1R as well as Lhx6 and/or PV, but not FoxP2. *In vitro* electrophysiological study revealed that, among 48 GP neurons, the SP agonist induced inward current in 21 neurons. The response was prevented by bath application of the NK-1R antagonist. Based on the firing properties, 92 recorded GP neurons were classified into three distinct types, i.e., CL1, 2 and 3. Interestingly, all the SP-responsive neurons were found to be in CL2 and CL3 types and, not in CL1. Moreover, active and passive membrane properties of the neurons in those clusters and immunofluorescent identification suggested that CL1 and CL2/3 could be considered as arkypallidal and prototypic neurons, respectively. Therefore, SP-responsive neurons were one of the populations of prototypic neurons based on both anatomical and electrophysiological results. Altogether, the striatal

direct pathway neurons could affect the indirect pathway in the way of prototypic neurons, via the action of SP to NK-1R.

Acknowledgement

I would like to express my sincere gratitude to my supervisor, Professor Fumino Fujiyama giving me this precious opportunity of the study as a Ph.D student in her laboratory. I especially would like to express my deepest appreciation to my supervisor, Dr. Fuyuki Karube for his elaborated guidance, considerable encouragement and invaluable discussion that lead to the accomplishment of my research.

I also extend my feelings of gratitude to my thesis reviewing committee: Dr. Yoshio Sakurai, Dr. Shigeo Takamori and Dr. Takeshi Sakaba, for their insightful comments and encouragement.

I am very grateful to Dr. Susumu Takahashi, Mr. Shinichiro Okamoto and other lab members for their valuable cooperation in my experiments.

Moreover, I thank Dr. Hiroyuki Hioki (Kyoto University) and Dr. Hiroshi Kameda (Teikyo University) for providing the PV／myrGFP-LDLRct transgenic mice.

Finally, I would like to extend indebtedness to my family and friends for their understanding, support, and encouragement throughout my study.

Table of contents

List of Figures and Tables

Figures

Tables

1. Introduction

1.1. Dual pathway of the basal ganglia

The basal ganglia are composed of; striatum (Str), globus pallidus (GP), entopedunucular nucleus (EP), subthalamic nucleus (STN), substantia nigra pars reticulata (SNr) and substantia nigra pars compacta (SNc). In the basal ganglia, several nuclei work in coordinated manner, and take on the planning and control of voluntary movement. Therefore, dysfunction of the basal ganglia causes motor dysfunction. Thus, it is important to examine the neural circuit of the basal ganglia in detail.

In the Str, the projection neurons are categorized into two groups, depending on their neurochemical properties and projection targets. The projection neurons transmit information via parallel and distinct routes to output nuclei, such as EP and SNr. The first projection group corresponds to a direct pathway, wherein the neurons express substance P (SP) and directly project to the output nuclei. The second projection group involves an indirect pathway, wherein the neurons express enkephalin and project to the output nuclei via the GP and the STN (Albin et al. 1989; Alexander and Crutcher 1990; Graybiel 1990). The classical models of the basal ganglia suggest that these dual pathways are independent of each other and work in an antagonistic manner to facilitate or inhibit movement, respectively (but see also Isomura et al. 2013; Cui et al. 2013). However, single-neuron tracing studies have revealed that almost all direct pathway neurons in rats (Kawaguchi et al. 1990; Fujiyama et al. 2011) and monkeys

(Lévesque and Parent 2005) projected to the GP, which is a relay nucleus of the indirect pathway.

A recent study on Drd1a-GFP and Drd2-GFP BAC transgenic mice revealed that the direct pathway collaterals directly inhibit the neurons in the GP (Cazorla et al. 2014). Although the GP is thought to primarily function as a relay nucleus of the indirect pathway of the basal ganglia (Albin et al. 1989; DeLong 1990; Smith et al. 1998; Obeso et al. 2008), these findings indicate that the direct pathway neurons drive not only the direct pathway but also the indirect pathway via the GP (Figure 1). Thus, the original conceptualization of the direct and indirect pathways should be modified through these recent studies, particularly that using in behavioral experiments.

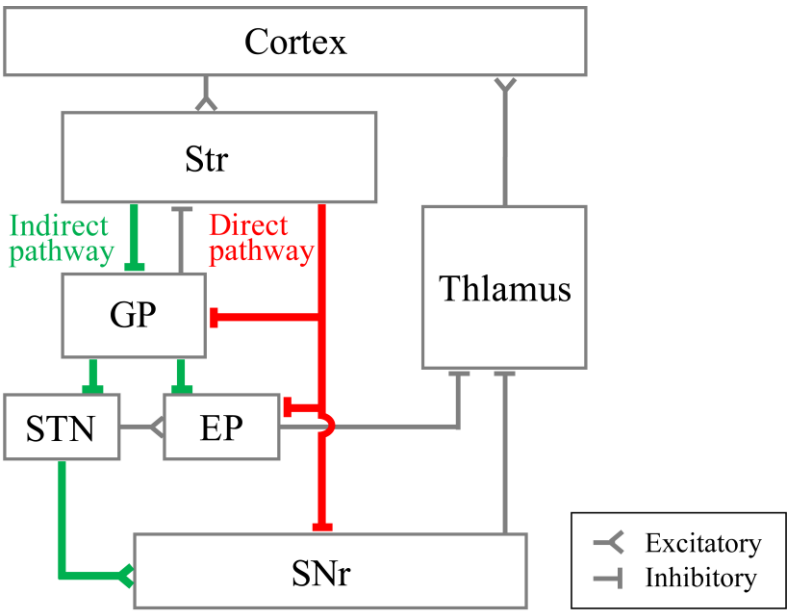

Figure 1. Schematic diagram of the direct and indirect pathways in the basal ganglia *Str* striatum; *GP* globus pallidus, *STN* subthalamic nucleus; *EP* entopeduncular nucleus; *SNr* substantia nigra pars reticulata

1.2. Dichotomous projection patterns of globus pallidus (GP) neurons

Many studies have revealed the cellular heterogeneity of the GP in terms of histochemical and electrophysiological properties or innervation patterns (Parent and De Bellefeuille 1983; Albin et al. 1989; Smith and Bolam 1989; Kita and Kitai 1994; Nambu and Llinas 1994; Mink 1996; Wichmann and Delong 1996; Nambu and Llinás 1997; Smith et al. 1998; Sato et al. 2000; Hoover and Marshall 2002; Nambu et al. 2002; Kita 2007; Sadek et al. 2007; Flandin et al. 2010; Gittis et al. 2014; Mastro et al. 2014; Abdi et al. 2015; Dodson et al. 2015; Fujiyama et al. 2015). In addition to the "prototypic" GP neurons that support uniform function by consistently innervating the STN (Bevan et al. 1998; Smith et al. 1998; Bevan et al. 2002; Kita 2007; Stephenson-Jones et al. 2011), single-cell labeling studies have revealed that a portion of prototypic neurons has both pallidostriatal and pallidosubthalamic collaterals (Mallet et al. 2012; Abdi et al. 2015; Fujiyama et al. 2015; Hernandez et al. 2015). However, another type of GP neurons, referred to as "arkypallidal" neurons (Mallet et al., 2012; Fujiyama et al., 2015), does not send descending axons toward STN; rather, purely innervates the striatum (Figure 2).

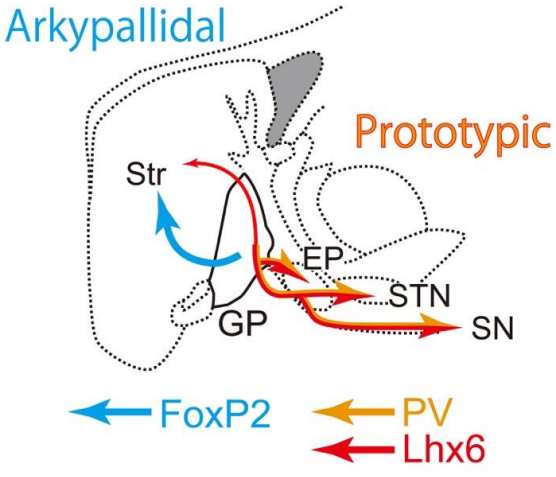

Figure 2. Prototypic and arkypallidal neurons in the globus pallidus (GP)
Two types of GP neurons classified by projection patterns and immunohistochemical properties. Prototypic neurons innervating the subthalamic nucleus (STN) co-expressed parvalbumin (PV) and/or Lim-homeobox 6 (Lhx6). In contrast, arkypallidal neurons expressed forkhead box protein P2 (FoxP2) and innervated the striatum (Str) but not STN.

The projection types also differed in terms of electrophysiological properties. In consistent with *in vitro* recording (Abdi et al. 2015; Hernandez et al. 2015), *in vivo* recording showed that prototypic neurons fired regularly at high rates than arkypallidal neurons in anesthetized (Abdi et al. 2015) or awake rats (Mallet et al. 2016) and mice (Dodson et al. 2015). Moreover, their activities were well correlated with animal behavior: arkypallidal neurons were active during spontaneous movement in mice (Dodson et al. 2015), whereas activities of prototypic neurons were heterogeneous; in rats, arkypallidal neurons were more strongly activated when the animal was forced to stop the planned movement (stop or cancellation task) than prototypic neurons were (Mallet et al. 2016). These electrophysiological and functional differences between GP prototypic and arkypallidal neurons could be associated with the differential inputs from striatal neurons. Cazorla et al. (2014; see their Fig. 4) showed that direct striatal neurons inhibited GP neurons heterogeneously and/or partially, whereas inhibition by the striatal indirect neurons was more intensive and homogeneous. It is, therefore, important to know which type of GP neurons is affected by the direct pathway collaterals.

1.3. How substance P (SP) effect in the GP?

Substance P is one of the neuropeptide called tachykinin released by the striatal direct neurons (Mantyh et al. 1984; Aosaki and Kawaguchi 1996; Shughrue et al. 1996; Furuta et al. 2004). Although there are three type of tachykinin receptor, SP has high affinity to the neurokinin-1 receptor (NK-1R). Previous studies showed that SP expressing axon terminals made apposition

with NK-1R expressing dendrites in the striatum (Aosaki and Kawaguchi 1996; Lee et al. 1997). Previous anatomical studies have reported the presence of NK-1R and NK-3R in the GP of rats (Mantyh et al. 1984; Elde et al. 1990; Gerfen 1991; Nakaya et al. 1994; Shughrue et al. 1996; Furuta et al. 2004) and humans (Mileusnic et al. 1999; Mounir and Parent 2002). It has been reported that only a few large-sized GP neuron express NK-1R. However, there were few reports for the NK-1R expressing neurons in the GP (see "Discussion"). Morphological evidence has accumulated that SP immunopositive terminals apposed with NK-1R-expressing neurons (Mounir and Parent 2002; Lévesque et al. 2006), and electrophysiological studies demonstrated that SP produced excitatory effects on the GP both *in vivo* (Cui et al. 2007) and *in vitro* (Chen et al. 2009). SP functions via metabotropic receptors and secondary messenger systems in the postsynaptic neurons, and this slow and more sustained response could also affect other neurotransmission, such as GABAergic inhibition.

It is known that half of the medium spiny neurons in the striatum possessed substance P as well as GABA. Further, previous works revealed that SP modified GABAergic transmission in the striatal local circuit and glutamatergic inputs from cerebral cortex or subthalamic nucleus (Blomeley and Bracci 2008; Govindaiah et al. 2010). Effects of SP on neurotransmission were also reported in other brain area: the nucleus tractus solitarius, nucleus accumbens, and amygdala (Maubach et al 2001; Kombian et al 2003; Bailey et al, 2004). Although it has been known that SP is located in the ascending cholinergic reticular system in rats (Vincent et al. 1983) and primates (Gomez-Gallego et al. 2007; Eid et al. 2016), only a

minority of cholinergic varicosities (17%) displayed a synaptic specialization in GP (Eid et al. 2016). Striatal direct neurons are known to possess the SP (Mantyh et al. 1984; Shughrue et al. 1996; Furuta et al. 2004) and give some collaterals in the GP (Kawaguchi et al. 1990; Lévesque and Parent 2005; Fujiyama et al. 2011; Cazorla et al. 2014). Taken together, the axon collaterals of the direct neurons are regarded as the most likely candidate as presynaptic elements to the NK-1R in the GP. Altogether, previous studies suggested that SP plays a role to modulate the GABAergic transmission by striatal axons in the GP.

Moreover, recent study also showed these striatal axon collaterals in GP inhibit the GP neurons in vivo (Cazola et al, 2014). Behavioral study showed that microinjection of SP into the GP affected on passive avoidance learning in rats (Kertes et al, 2009). Then, I hypothesized that the SP released by striatal direct pathway neurons might contribute to the modulation of neurotransmission on GP neurons via the NK-1R.

In the present study, I aimed at elucidating how and what types of neurons in the GP are affected by SP, presumably released by striatal direct neurons. To this end, I first identified the characteristics of NK-1R neurons using a combination of fluorescent retrograde labeling with immunofluorescence staining. I then made whole cell patch–clamp recording in slice preparations and found that SP affected GP neurons in a highly cell type-selective manner.

This study has been reported in the journal named Brain Structure and Function (Mizutani et al. 2017; fast online published).

2. Materials and Methods

All animal experiments were approved and performed in accordance with the guidelines for the care and use of laboratory animals established by the Committee for Animal Care and Use and that for Recombinant DNA Study of Doshisha University. All efforts were made to minimize animal suffering and the number of animals used. Chemicals were derived from Nacalai Tesque (Kyoto, Japan) and Wako (Osaka, Japan), unless otherwise noted.

Double or Triple immunofluorescence labeling

Male mice (C57BL/6J, postnatal (P) 7–12 weeks, N = 12; P 21 days, N = 2) were deeply anesthetized with isoflurane (Pfizer Japan Inc., Tokyo, Japan) and sodium pentobarbital (100 mg/kg, i.p.; Kyoritsu Seiyaku Corporation, Tokyo, Japan). The mice were then transcardially perfused with 8.5% sucrose in 20 mM phosphate buffer (PB) containing 1 mM $MgCl_2$, followed by 4% w/v paraformaldehyde and 75% saturated picric acid in 0.1 M PB. After perfusion pump off, the brain was postfixed *in situ* for 1.5 h at room temperature (RT), and then the brain was removed from the skull followed by cryoprotection with 30% sucrose in phosphate-buffered saline (PBS) for 24 h at 4℃. Tissue blocks containing the GP were sectioned sagittally using a freezing microtome (Leica Microsystems, Wetzlar, Germany) at a thickness of 25 μm. Floating sections were collected in six series and prepared for immunofluorescence to reveal GP molecular markers as listed in Table 1 (cf. Mallet et al. 2012; Abdi et al. 2015). The sections were incubated with a mixture of primary antibodies

(Table 1) for overnight at 4°C. The primary antibodies were diluted with incubation buffer containing 10% (v/v) normal donkey serum (Merck KGaA, Darmstadt, Germany), 2% bovine serum albumin and 0.5% (v/v) Triton X-100 in 0.05 M Tris-sbuffered saline (TBS). After exposure to the primary antibodies, the sections were washed in PBS and incubated for 5 h at RT in the same buffer containing a mixture of secondary antibodies that were conjugated to the fluorophores (Table 2).

Table 1. Primary antibodies used for research purposes

Antigen	Host Species	Dilution	Supplier	Catalog no.
NK-1R (rat; C-terminus: 393-407 AA)	Guinea Pig	1:2000	Merck KGaA (Darmstadt, Germany)	AB15810
NK-1R *(rat; C-terminus: 385-407 AA)	Rabbit	1:2000	Merck KGaA	AB5060
NK-1R (rat; C-terminus: 393-407 AA)	Rabbit	1:1000	Sigma Aldrich (St. Louis, MO)	S8305
NK-1R (rat; the second extracellular loop: 180-194 AA)	Rabbit	1:100	Alomone Labs (Jerusalem, Israel)	ATR-001
NK-3R	Rabbit	1:1000	Immunostar (Hudson, WI)	20061
NeuN	Mouse	1:15000	Merck KGaA	MAB377
NeuN	Rabbit	1:4000	Merck KGaA	ABN78
PV	Mouse	1:4000	Sigma Aldrich	P3088
PV	Guinea Pig	1:5000	Synaptic Systems (Goettingen, Germany)	195004
PV	Rabbit	1:4000	Immunostar	24428
Lhx6	Mouse	1:500	Santacruz (Dallas, Tex)	sc-271433
FoxP2	Rabbit	1:2000	Abcam (Cambridge, UK)	ab16046
FoxP2	Goat	1:1000	Santacruz	sc-21069
ChAT	Mouse	1:5000	Merck KGaA	MAB305

*, the antibody was firstly used for preliminary experiments, but soon Merck KGaA stopped to product it. Therefore, the antibody was not used to obtain the results, and not verified for reliability.

Table 2. Secondary antibodies used in research

Secondary Antibody	Host Species	Dilution	Supplier	Catalog no.
Anti-mouse Alexa Fluor®350	Donkey	1:500	Thermo Fisher Scientific, Inc. (Waltham, MA)	A10035
Anti-mouse Alexa Fluor®546	Donkey	1:500	Thermo Fisher Scientific, Inc.	A10036
Anti-mouse Alexa Fluor®488	Donkey	1:500	Thermo Fisher Scientific, Inc.	A21202
Anti-mouse Alexa Fluor®594	Goat	1:500	Thermo Fisher Scientific, Inc.	A11032
Anti-mouse Alexa Fluor®635	Goat	1:500	Thermo Fisher Scientific, Inc.	A31575
Anti-guinea pig Alexa Fluor®488	Goat	1:500	Thermo Fisher Scientific, Inc.	A11073
Anti-guinea pig Alexa Fluor®594	Goat	1:500	Thermo Fisher Scientific, Inc.	A11076
Anti-guinea pig CF350	Goat	1:500	Biotium (Fremont, CA)	20198
Anti-rabbit Alexa Fluor®488	Donkey	1:500	Thermo Fisher Scientific, Inc.	A21206
Anti-rabbit Alexa Fluor®488	Goat	1:500	Thermo Fisher Scientific, Inc.	A11034
Anti-rabbit Alexa Fluor®594	Goat	1:500	Thermo Fisher Scientific, Inc.	A11037
Anti-rabbit Alexa Fluor®635	Goat	1:500	Thermo Fisher Scientific, Inc.	A31577
Anti-rabbit CF594	Goat	1:500	Biotium	20113
Anti-goat Alexa Fluor®594	Donkey	1:500	Thermo Fisher Scientific, Inc.	A11058

After rinsing, the sections were mounted on to glass slides, air dried and cover-slipped with 50% (v/v) glycerol/TBS. Immunofluorescence was observed under an epifluorescent microscope (BX-53, Olympus, Tokyo, Japan) or a confocal microscope (FV1200, Olympus) with appropriate filter sets (359–371 nm excitation and ≥397-nm emission for AlexaFluor (AF) 350; 450–490-nm excitation and 514–565-nm emission for AF488; 530–585-nm excitation and 575-675-nm emission for AF594; 590–650 nm excitation and 655-675-nm emission for AF635). The images of each of the channels were taken sequentially and separately to negate possible crosstalk of signals across channels. The images of the immunofluorescence were captured with 10x, 40x, 60x or 100x objective lens with the respective software (cellSens for BX-53 or FLUOVIEW for FV1200, Olympus). One focal image was taken from each view and a montage view of the whole GP was created. I defined the GP area according to relative location with other brain structures (Fig. 11a). Only the immunoreactive neurons in focus were counted without a stereological method. Additionally, since NK-1R is a receptor located in the plasma membrane, I investigated the intracellular distribution of the immunofluorescence using a confocal microscope (Fig. 12).

Evaluation of NK-1R immunoreactivity

To verify the specificity of the NK-1R antibody (Merck AB15810; Table 1), I used two different antibodies against the C-terminal amino acid sequence (Fig. 6). The immunogen of one antibody (**a**, Merck KGaA AB15810) is COOH-terminus (393-407 amino acids). The

immunogen of other two antibodies is a synthetic peptide that corresponds to the COOH-terminus of the NK-1R (**b**, 385-407 amino acids, Merck KGaA AB5060; **c**, 393-407 amino acids, Sigma-Aldrich S8305).

Moreover, I also examined another antibody against the amino acid sequence of the NK-1R second extracellular loop (Alomone Labs ATR-001, Jerusalem, Israel) was also examined (Fig. 7, Fig. 13h, I and Table 1). Two antibodies against different amino acid sequences of the NK-1R peptide detected immunoreactive neurons in a similar manner. One antibody was raised against the second extracellular loop (2nd loop) of the NK-1R peptide (Alomone Labs ATR-001) and another antibody against the C-terminus of the NK-1R peptide (Merck KGaA AB15810).

To further confirm whether the fluorescent signals detected by Merck AB15810 and Alomone Labs ATR-001 were specific for their antigen, I carried out a pre-absorption test (Fig. 8). For Merck AB15810, a synthetic peptide (Abcam, AB92810, Cambridge, UK) corresponding to the C-terminus of NK-1R (amino acid sequence 393-407: KTMTESSSFYSNMLA) was used. The antibody (~1 μg/ mL for final working concentration) was mixed with an excess amount of the peptide (20- or 200-fold in mol) in usual incubation buffer for 12 h at 4 °C. Then mouse brain sections were incubated with the pre-absorbed antibody, followed by incubation with the secondary antibody (Alexa 488 conjugated antibody; Thermo Fisher Scientific, Waltham, MA, USA). **A**n NK-1R antibody (Merck KGaA, AB15810) was pre-incubated with a 20- or 200- fold (in mol) amount of the NK-1R C-terminus peptide (Abcam, AB92810) for 12h before incubation with brain sections. Photo images for immunofluorescent by untreated or pre-

absorbed antibodies were taken under the same conditions (exposure time, 1 second). Another NK-1R antibody (Alomone Labs ATR-001) was pre-incubated with a 200-fold amount (in mol) of the antigen peptide (Alomone Labs) for 12h before incubation with brain sections. Photo images for immunofluorescent by untreated or pre-absorbed antibodies were taken under the same conditions (exposure time, 0.91 seconds). Finally, I also investigated NK-1R messenger RNA expression by *in situ* hybridization (Fig. 9) to compare with protein expression detected by immunofluorescence in collaboration with Mr. Shinichiro Okamoto. The following hybridization procedure was carried out as reported previously (Hioki et al. 2010; Ma et al. 2011). Briefly, sagittal sections from both hemispheres were cut at 20 μm thickness using a freezing microtome. Free floating sections were hybridized for 16-20 h at 60℃ with 1 μg/mL digoxigenin (DIG)-labeled sense or antisense riboprobes in a hybridization buffer. After washes and ribonuclease A (RNase A) treatment, the sections were incubated overnight with 1:1000 diluted alkaline phosphatase (AP)-conjugated anti-DIG sheep antibody (11-093-274-910; Roche Diagnostics) and then reacted with 0.375 mg/mL nitroblue tetrazolium and 0.188 mg/mL 5-bromo-4-chloro-3-indolylphosphate (NBT/BCIP; Roche Diagnostics) for several hours (Hioki et al. 2010). Sense probes detected no signal higher than the background. To enhance the signals for NK-1R mRNA sensitively, we applied BT-GO amplification method (Furuta et al. 2009; Kuramoto et al. 2009; Ge et al. 2010). Briefly, after hybridization with DIG-labeled NK-1R riboprobe, the sections were incubated with 1:4000 diluted peroxidase-conjugated anti-DIG sheep antibody (11-207-733-910; Roche Diagnostics). Subsequently, the sections were reacted

with a mixture containing 25 µM of BT, 3 µg/mL of GO, 2 mg/mL of beta-D-glucose and 2% bovine serum albumin in 0.1 M PB for 30 min. We used BT at a concentration either of 0.25, 2.5, or 25 µM. The sections were further incubated with 1:1000 diluted AP-conjugated streptavidin (02516-71; nacalai tesque) for 2 h and finally reacted with NBT/BCIP. Each of the four probes (target sequence position; 15-895, 2013-2734, 3222-3827, 993-1970; GenoStaff, Minoh, Japan) exhibited very similar expression patterns for mouse brains.

Combined fluorescent retrograde labeling with immunofluorescence staining

Male and female mice (C57BL/6J, P 8–10 weeks, N = 5) were anesthetized by inhalation of isoflurane and intramuscular injection of a mixture of 40 mg/kg ketamine (Ketalar; Daiichi-Sankyo, Tokyo, Japan) and 4 mg/kg xylazine (Bayer HealthCare, Berlin, Germany). The mice were then fixed to the stereotaxic device (Narishige, Tokyo, Japan) and the skull was drilled to make a small hole in an appropriate anteroposterior (AP) and lateromedial (LM) position in accordance with the mouse brain atlas (Paxinos and Franklin, 2013). For retrograde labeling, 1.0% Alexa Fluor 555-conjugated cholera toxin subunit B (CTB555; Thermo Fisher Scientific, Waltham, MA, USA) or 2.5% Fast Blue (FB; Polysciences, Inc. Warrington, PA, USA) was injected into the STN (AP 1.6 mm caudal from the bregma, LM 1.68 mm from the midline, depth 4.8 mm from the pial surface) or striatum (AP 1.3 mm rostral from the bregma, LM 1.68 mm from the midline, depth 3.0 mm from the pial surface), respectively, through a glass pipette (~20 µm of tip diameter) by 20 psi for 10–40 ms of air pulses (PV820, World Precision

Instruments, Sarasota, FL, USA). Following a survival period of 3–4 days, the animals were perfused and tissue was prepared as described above. For the count of STN-projecting cells, I carefully excluded the anterograde-labeling terminals originating from STN and selected only retrogradely labeled STN-projecting GP neurons (for an example of false labeling forming cell-like shape, see Fig. 3).

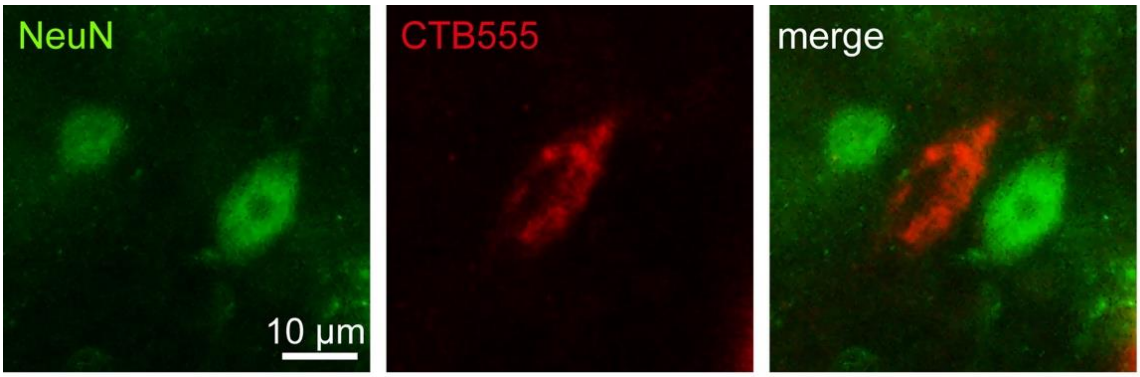

Figure 3. Anterograde labeling of CTB555 formed cell-like shape.
Injection of Alexa Fluor 555-conjugated cholera toxin subunit B (CTB555; *red*) into the subthalamus retrogradely labeled pallidosubthalamic neurons in the GP, as shown in Fig. 15; however, false positive cell-like shape of labeling (*red*; center of the image) was occasionally observed as shown here, lacking NeuN immunoreactivity (*green*). Note that the anterogradely labeled terminals originating from subthalamus did not overlap with NeuN immunofluorescence.

in vitro electrophysiological recording

Thirty-one mice [C57BL/6J and PV/myrGFP-LDLRct transgenic strains (Kameda et al. 2012)] were used for slice recording at P17–27 days. Since green fluorescent protein (GFP) is introduced in parvalbumin (PV) neurons in PV/myrGFP-LDLRct mice, they are suitable to target PV neurons. In total 69 neurons were recorded from C57BL/6J, 8 neurons from the transgenic mice, and 15 neurons from wild-type littermates of the transgenic line. Data were

pooled because no difference was observed among lines. They were deeply anesthetized with sodium pentobarbital and the brain was taken out and soon immersed in ice-cold ACSF (NaCl 125; KCl, 2.5; $CaCl_2$, 2.4; $MgCl_2$, 1.2; $NaHCO_3$, 25; glucose, 15; $NaHPO_4$, 1.25; pyruvic acid 2; lactic acid 4; in mM) for 2 min. All ACSFs were aerated with 95%/5% O_2/CO_2 continuously. Three hundred-micrometers thick-sagittal slices were cut by a vibratome (Leica VT-1000, Leica Microsystems) and incubated with the ACSF at 32°C for 20 min, and then the chamber was transferred to RT. At least after 1h of recovering, the slice was moved into a recording chamber (30°C). A whole cell glass pipette (4–7MΩ) was filled with intracellular solution (K-methylsulfate 126; KCl 6; Na_2ATP 4; NaGTP 0.3; $MgCl_2$ 2; Na_4EGTA 0.6; HEPES 10; biocytin 20.1; in mM). The pH was adjusted to 7.3 by KOH and the osmolality to ~290 mOsm. The GP was identified under IR-DIC configuration. Current or voltage clamp recordings were low-pass filtered at 3 kHz and recorded using EPC10 (HEKA Elektronik Dr. Schulze GmbH, Lambrecht/Pfalz, Germany) with a sampling rate of 20 kHz. Once the cells were recorded in a whole cell voltage clamp mode, the series resistance was repeatedly monitored by applying a brief voltage pulse (–5 or –10 mV for 10 ms), and if the series resistance was beyond 20 MΩ, the record was omitted from the further analysis. Shortly (less than 1 min) after the accomplishment of whole cell configuration, the firing responses against 1 s of depolarizing current pulses (the maximum intensity was 950 pA increasing with a 50 pA step) were recorded in a current clamp mode. Then passive membrane properties were monitored by steps of 1 s of hyperpolarized current pulses application. NK-1R agonist ([Sar^9, $Met(O_2)^{11}$]-SP;

Sigma-Aldrich, St. Louis, MO, USA), hereafter referred to as SM-SP, was solved with aerated ACSF (0.1 or 1 mM) and filled in another electrode. The SM-SP electrode was placed close to the recorded soma, and SM-SP was applied to the recorded GP neuron using a precision pressure control and valve system (5–10 psi for 10–110 ms by a PV820 picopump). If the recorded cells did not respond to a 10 ms of SM-SP puff, the puff duration was gradually increased up to 110 ms to define whether the neuron responded to SM-SP or not. The SM-SP-induced responses were monitored either in a current or voltage clamp mode. I tested responses against SM-SP in 48 GP neurons from 31 mice. During voltage clamp recording, the holding potential was usually set at –50 mV, which was close to the average membrane potential of our samples of GP neurons (Table 3). Then, the holding potential was shifted from –40 to –70 mV to investigate voltage dependence of SM-SP responses (N = 5 neurons). For seven neurons, a cocktail of glutamate and GABA receptors antagonists was applied in a bath (CNQX, 10 μM; D-AP5, 20 μM; SR95531, 20 μM). For two SM-SP-responsive neurons, NK-1R antagonist (SR140333) was applied in bath solution and then re-examined on an effect of an SM-SP agonist puff. Those pharmacological reagents were purchased from Tocris Bioscience (Bristol, UK).

Tissue cleaning method to intensify immunofluorescent detection in slice preparation

To clarify NK-1R immunofluorescence in 300-μm-thickness slices, I applied one of the tissue cleaning methods, AbScale (Hama et al. 2015). See the reference for the detailed method. In

brief, slices were fixed with a fixative composed of 4% paraformaldehyde, 0.2% picric acid, and 0.05% glutaraldehyde (GA) in 0.1M PB for 4h at RT and then the fixative without GA for overnight. After rinse with PBS(–) for 3h, incubation with (1) ScaleS0 (~6h, 37°C); (2) ScaleA2 (~24h, 37°C); (3) ScaleB4(0) (~12h, 37°C); (4) ScaleA2 (~6h, 37°C); (5) AbScale with primary antibodies (~24 to 48h, 37°C); (6) rinse with AbScale twice (1h for each, RT); (7) AbScale with secondary antibodies and CF dye-conjugated streptavidin (Biotium, Fremont, CA, USA) (~24 to 48h, 37°C); (8) rinse with AbScale twice (4h, RT); (9) rinse with 'AbScale rinse' twice (2h for each, RT); (10) refixation with 4% paraformaldehyde in PB; (11) rinse with PBS(–) for 1h at RT; (12) ScaleS4 (~6h, 37°C); (13) ScaleS4 (~12h, 37°C); (14) mounting with ScaleS4. The dilution of antibodies was the same as other immunoreaction (Table 1). The composition of solutions was the same as Supplementary Figure 2 of Hama et al. (2015). The mounted samples were observed with a confocal microscope.

Analysis of electrophysiological data

The analysis was performed by IgorPro (Wave Metrics Inc., Portland, OR, USA) using Neuromatic plugin (http://www.neuromatic.thinkrandom.com). All of the recording data were smoothed with a 0.2-ms moving time window corresponding to the moving average of four consecutive recording points. The input resistance (R_{in}) was determined by linear fitting of voltage responses to hyperpolarized current pulses injection (–20 to –100 pA by –20 pA steps). The membrane time constant (tau) was calculated from the responses to a –200 pA current

pulse by fitting the rising phase with an exponential curve. Hyperpolarizing sag potential induced by –200 pA pulse was measured as the voltage difference between the negative peaks of the exponential fit of the rising phase and that of the actual membrane potential. To define action potential threshold, membrane voltage trace including the action potential elicited by the minimum intensity of a depolarizing pulse was differentiated twice to obtain [(d*V*/d*t*)/d*t*]. The time point of the positive peak of [(d*V*/d*t*)/d*t*] just prior to the action potential peak was defined as the spike onset, and the membrane potential at that timing as the threshold. The full width of the spike was measured at the voltage level of the threshold. The amplitude of fast and slow after hyperpolarization (fAHP and sAHP) was measured from the threshold to the hyperpolarized peak potential. fAHP or sAHP delay was defined as the duration between the peak of the action potential and the peak of the following AHP. Our definition of the above parameters is summarized in Figure 4.

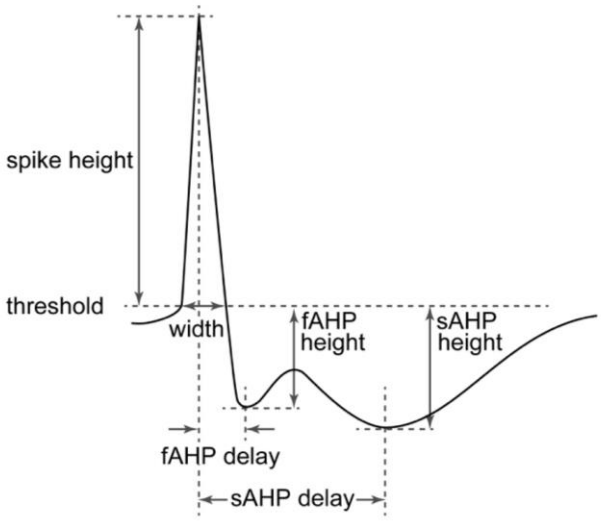

Figure 4. Schematic representation of electrophysiological parameters described in our present study. fAHP, fast after hyperpolarization; sAHP, slow after hyperpolarization.

To quantify SM-SP-evoked responses, the ten sweeps stimulated by SM-SP were acquired and aligned with the SM-SP air puff onset on both time and membrane potential, and then the

average trace was calculated. If the peak amplitude of the SM-SP-evoked response of the averaged trace was three times larger than the standard deviation (SD) of the pre-stimulus period (50–250 ms in duration), the neuron was defined as SM-SP responsive. Since I varied the concentration of SM-SP and air puff duration, the amplitude of SM-SP-evoked responses was not compared quantitatively across neurons. SM-SP-evoked charge was calculated from the average trace during 1-s period from the end of SM-SP puff. To quantify voltage dependence of SM-SP response in a single neuron, the SM-SP-evoked current amplitude and charge at each holding potential were normalized by the maximum amplitude (Fig. 17). Statistical analysis was conducted by IgorPro and R (http://www.r-project.org/; R Project for Statistical Computing, Vienna, Austria). Data were described as mean ± SD, except for otherwise noted. Cluster analysis was conducted onto four electrophysiological parameters: spike width, spike threshold, spike frequency at 100 pA depolarized pulse, and the maximum spike frequency. Each parameter was normalized as (value – mean)/SD, resulting in the mean of a normalized parameter equal to 0 and their SD to 1. Then the Euclidean distance between samples was calculated and the square of the distance was used for the cluster analysis with the Ward method (Ward 1963). Statistical significance of comparison among clusters was first examined by one-way ANOVA followed by Tukey test for multiple comparisons. The difference in the proportion of neurons was proven by pairwise comparison test with *p* value correction by Holm's method.

3. Results

It has been reported that the direct pathway neurons give axon collaterals to the GP. However, it is not clear how and which type of GP neurons are affected by the direct pathway neurons. Because the direct pathway neurons contain the substance P, I thought the substance P and NK-1R, the principal receptor of the substance P, were the clue of the question. I performed the following morphological and electrophysiological approaches to clarify how and which GP neurons are affected by SP.

3.1. Expression of neurokinin-1 receptor (NK-1R) in the GP

It has been reported that only a few GP neurons express NK-1R by immunohistochemistry (Nakaya et al. 1994; but see also Chen et al. 2009) or *in situ* hybridization (Elde et al. 1990; Gerfen 1991; Allen Institute mouse brain atlas: http://mouse.brain-map.org/; see also Fig. 9). However, I observed that 38.9% of GP neurons showed NK-1R immunoreactivity (Fig. 5) with an antibody (Merck KGaA AB15810) which recognizes the C-terminus of NK-1R. Surprisingly, the number of NK-1R immunoreactive neurons was much higher than previous reports. Additionally, I found new type of NK-1R immunoreactive GP neurons which showed relatively moderate NK-1R expression than the neurons previously reported (Fig. 5a_2, b).

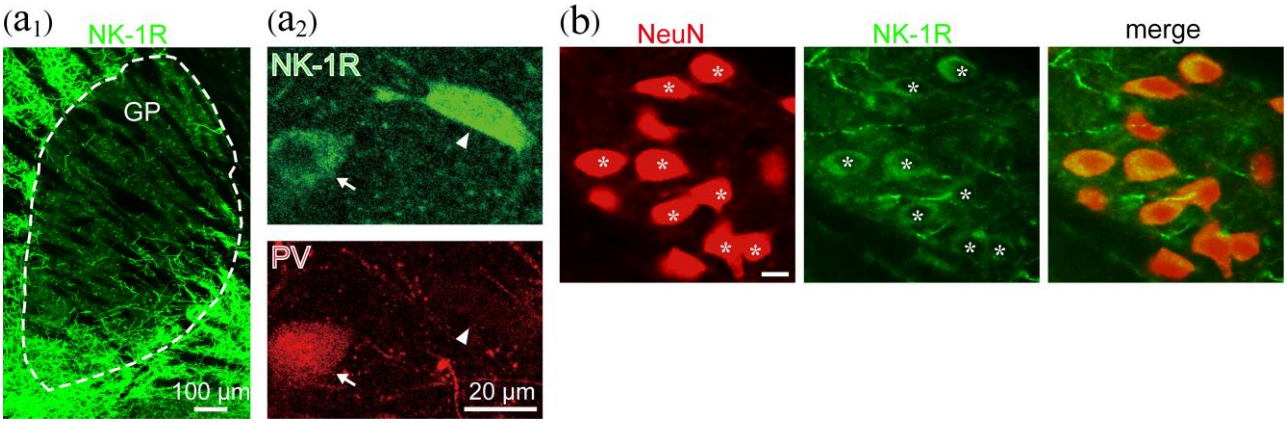

Figure 5. Two types of neurokinin-1 receptor (NK-1R) immunoreactivity in the GP
a1 A photomicrograph of GP showing NK-1R immunoreactivity (*green*). **a2** Two types of NK-1R immunoreactive neurons in GP. *Upper*, dense labeling for NK-1R was always observed in a neuron possessing a large cell body (*arrowhead*). Dendrites were also densely labeled. On the contrary, a relatively small neuron was stained bit faintly, lacking label in dendrites (*arrow*). *Bottom*, a large NK-1R neuron did not express PV (*arrowheads*), but a small NK-1R neuron was PV-immunopositive. The section was processed using AbScale.
b Magnified image of the GP showing double immunofluorescence labeling for NeuN (*red*) and NK-1R (*green, asterisks*). *Scale bar* 10 μm.

To verify the moderate NK-1R immunoreactive GP neurons, I have tried following experiments. First I used three different antibodies against the C-terminal peptide sequence of NK-1R, and observed the immunoreactivity in some nucleus of the central nerve system. Similar immunofluorescence was also observed by other two antibodies against the C-terminal amino acid sequences of the NK-1R peptide (Sigma-Aldrich S8305, St. Louis, MO; Merck KGaA AB5060; Fig. 6; see also Table 1).

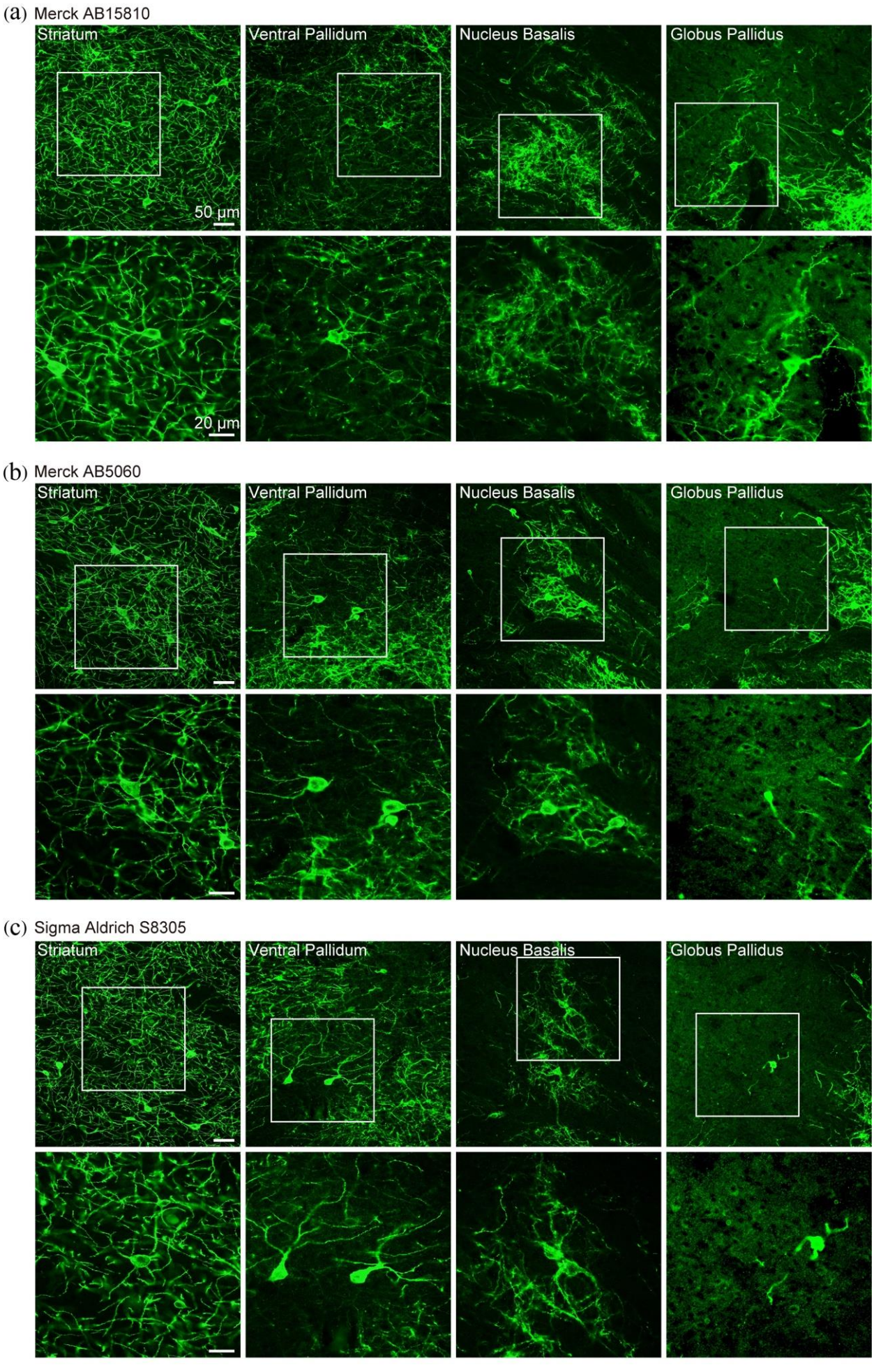
(a) Merck AB15810
Striatum
Ventral Pallidum
Nucleus Basalis
Globus Pallidus
50 µm
20 µm
(b) Merck AB5060
Striatum
Ventral Pallidum
Nucleus Basalis
Globus Pallidus
(c) Sigma Aldrich S8305
Striatum
Ventral Pallidum
Nucleus Basalis
Globus Pallidus

Figure 6. NK-1R immunoreactivity with three different antibodies against the C-terminus peptide sequences.
Photo images of NK-1R immunoreactivity (AF488) were taken from the striatum, ventral pallidum, nucleus basalis, and GP. Immunofluorescence with three antibodies (**a**, Merck KGaA AB15810, **b,** Merck KGaA AB5060, **c**, Sigma-Aldrich S8305) resulted in similar images. Note that strong immunopositive NK-1R neurons are surrounded by weak immunopositive NK-1R neurons in GP with any antibodies.

I also examined another NK-1R antibody which was raised against a different amino acids portion of the NK-1R (Alomone Labs ATR-001; Table 1). Double immunofluorescent labeling revealed Merk KGaA AB15810 and Alomone Labs ATR-001 detected almost the same population of GP neurons (Fig. 7, Fig. 13h, i; for details, see "Materials and Methods"). I found that these two antibodies showed similar immunoreactivity on cell bodies for both strong and moderate labeling. The results indicated both intensive and moderate signals were specific for the antigen, and denied a non-specific binding of the antibody. Indeed, among 141 GP neurons labeled by Alomone Labs ATR-001, 128 neurons (90.8%) were also labeled by Merck AB15810. Conversely, Merck AB15810 detected 132 GP neurons, among which 128 neurons (97.0%) were also labeled by Alomone Labs ATR-001 (Fig. 7).

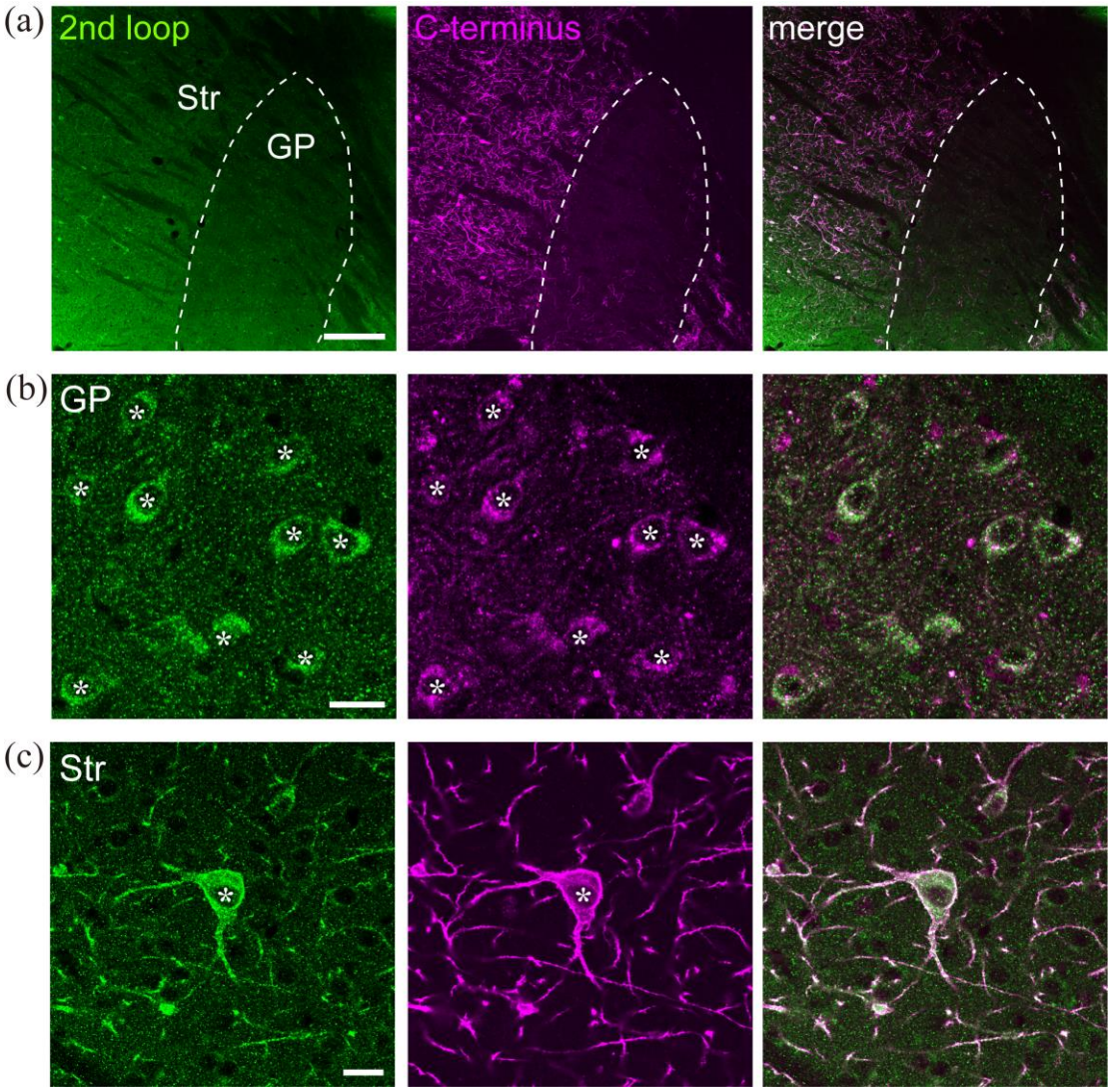

Figure 7. Two antibodies against different amino acid sequences of the NK-1R peptide detected immunoreactive neurons in a similar manner.
a Low magnification images of the striatum (Str) and GP. The immunofluorescence by two antibodies overlapped with each other in the GP (**b**, *right*) and the striatum (**c**, *right*). Immunoreactive neurons were marked with *asterisks*. *Scale bar* 50 μm for **a**; 20 μm for **b**, **c**

Pre-absorption test also showed specificity of Merck AB15810 for the NK-1R. As the result, immunofluorescence by Merck AB15810 was completely disappeared by pre-absorption with the 200-fold amount of peptide, whereas immunofluorescence was still observed by absorption with the 20-fold amount of peptide (Fig. 8). Notably, the presence of strong immunoreactivity in

the striatum and in large (putative cholinergic) neurons in the GP was always accompanied with that of relatively moderate or weak immunofluorescence in small neurons in the GP. A pre-absorption test on the Alomone Labs ATR-001 also diminished immunofluorescence (Fig. 8, Table 1).

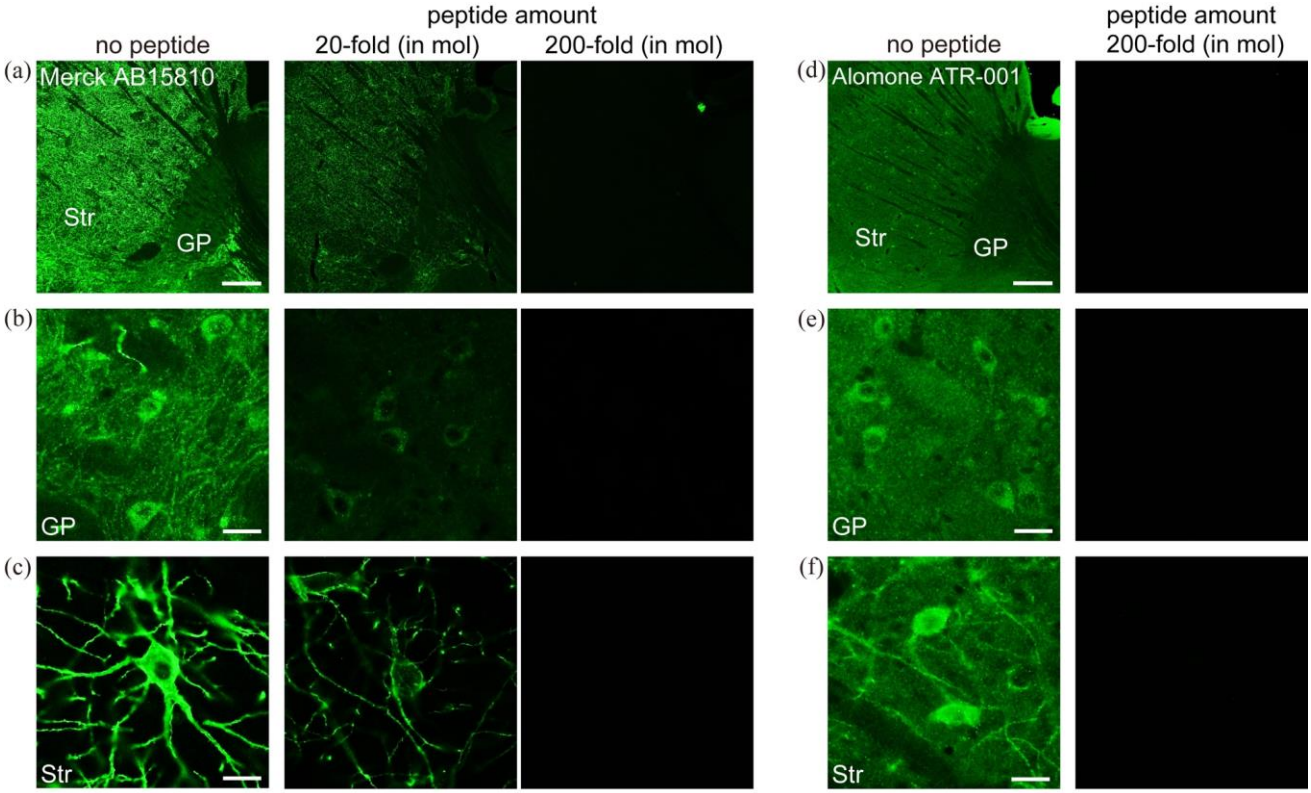

Figure 8. Pre-absorption tests for two NK-1R antibodies using synthetic antigen peptides.
a A low magnification image of the striatum (Str) and GP. The no-absorbed antibody revealed immunoreactive neurons in the GP (**b**, *left*) and Str (**c**, *left*). **d** A low magnification image of the Str and GP. Magnified images of the GP; **e** and Str; **f** indicated immunoreactive neurons detected by the non-absorbed antibody (*left*). Again, the pre-absorbed antibody did not visualize any neurons (*right*). *Scale bar* 100 μm for **a**, **d**; 20 μm for **b**, **c**, **e**, **f**.

Evaluation test for the NK-1R antibodies indicated that both intensive and moderate signals were specific for the antigen, and denied a non-specific binding of the antibodies. These results

strongly supported that in the basal ganglia including GP, immunofluorescence method could detect relatively lower level expression of NK-1R, in addition to well-known strong NK-1R expression observed in the striatum.

I also investigated NK-1R messenger RNA expression. In our study, however, *in situ* hybridization did not provide conclusive evidence of the weak or moderate signals in the GP (Fig. 9). I discuss the discrepancy between immunofluorescence and *in situ* hybridization in "Discussion". I found that there is similar moderate NK-1R immunoreactivity in SNr. However, mRNA expression was not observed in SNr as same as in GP. Data shown in figure 9 were derived from a probe of 993-1970 nucleic acid sequence, just the same as used in Allen Institute atlas #1296 (data not shown for other three probes), validating the reproducibility of the *in situ* hybridization result.

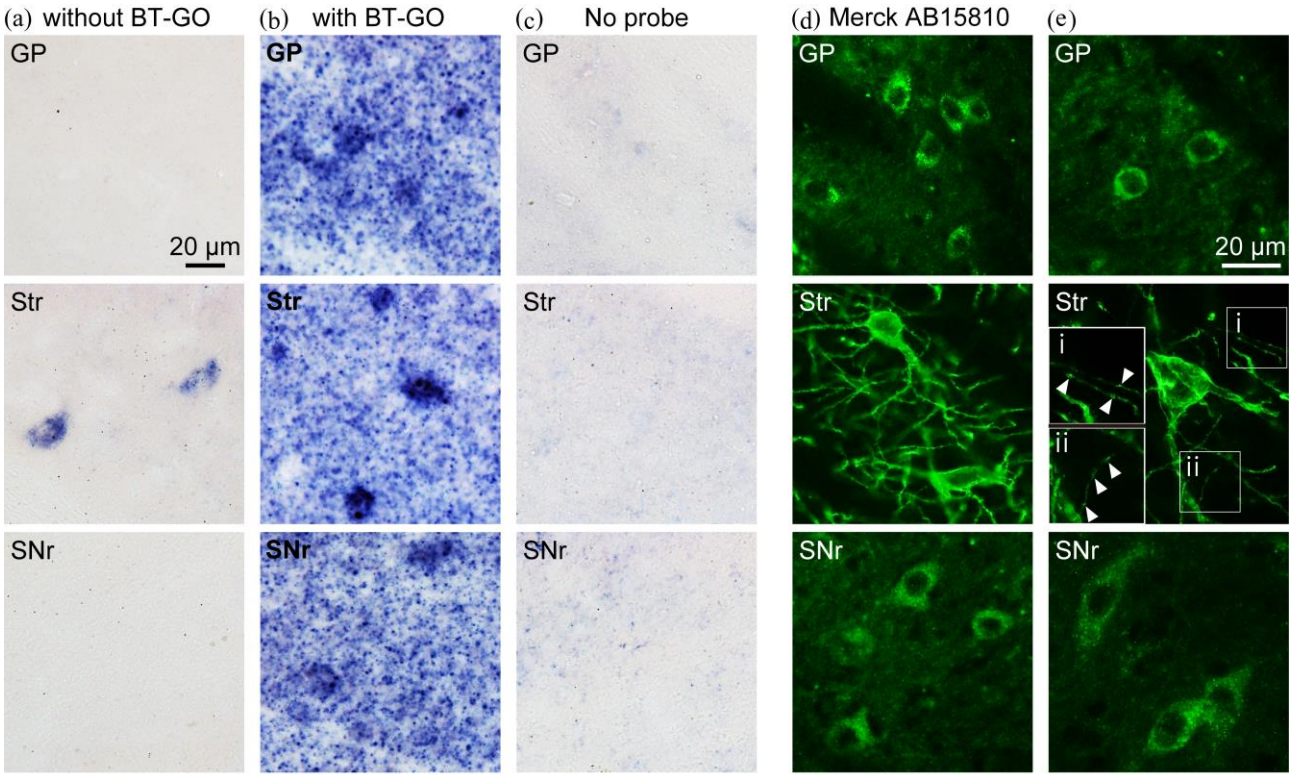

Figure 9. Localization of NK-1R mRNA expression in the striatum (Str), GP and substantia nigra pars reticulata (SNr).
Localization of NK-1R mRNA expression in the globus pallidus (GP) and striatum (Str) without **a** or with **b** biotinylated tyramine-glucose oxidase (BT-GO) amplification (see below). Note that strong NK-1R signals were observed in the striatum (**a**, *middle*). No signal was detected in the GP (**a**, *top*) and SNr (**a**, *bottom*) without amplification. **b** BT-GO amplification produced additional faint staining in the GP and SNr; however, it was hard to distinguish actual signals from the background. **c** No neuron-like signal was observed in the control sections (No probe). **d** For comparison, photo images of NK-1R immunofluorescence (Merck AB15810) were shown at the same magnification with those of *in situ* hybridization. In SNr, some neurons were labeled by the NK-1R antibody. **e** Magnified multi-focus images of NK-1R immunofluorescence. Note that almost only cell bodies and thick dendrites were labeled in GP (*top*) and SNr (*bottom*), whereas in the striatum (*middle*), a number of neurites were also labeled. Boxed areas **i** and **ii** were shown in higher magnification in *insets*. Thin neurites with puncta (*arrowheads*) were clearly labeled.

3.2. NK-1R immunoreactivity showed different representation from NK-3R in the GP

Previous study showed that strong NK-1R immunoreactive neurons did not co-express NK-3R, one of the subtypes of the neurokinin receptors, in the GP (Furuta et al. 2004). On the other hand, other research reported the coexistence of NK-1R and NK-3R in the same dendrites of GP neurons using electron microscope (Lévesque et al., 2006). In this study, I examined whether NK-1R neurons co-expressed NK-3R or not.

Double immunofluorescence labeling for NK-1R and NK-3R showed that the strong immunopositive NK-1R neurons showed weak NK-3R immunoreactivity (Fig. 10).

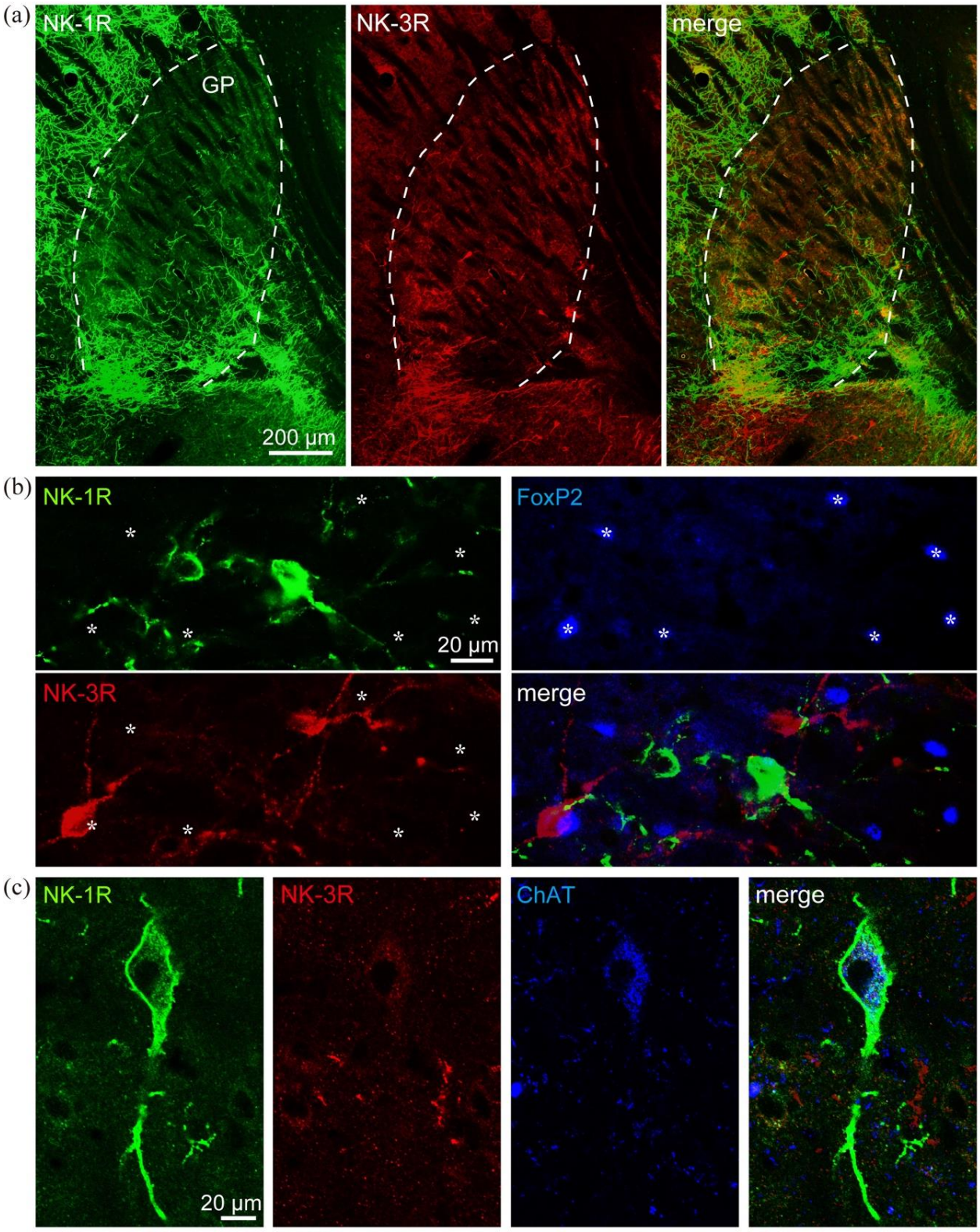

Figure 10. Triple immunofluorescent labeling for NK-1R, NK-3R and choline acetyltransferase (ChAT) or FoxP2 in GP.
a Low magnification images of immunofluorescence for NK-1R (*green*) and NK-3R (*red*). Note dense staining of NK-1R and NK-3R was segregated from each other (see *merge* image). **b** FoxP2 neurons, arkypallidal neurons (*blue, asterisks*), co-expressed neither NK-1R nor NK-3R. Strong NK-1R (*green*) and NK-3R (*red*) immunoreactions were observed in non-overlapping populations.

c Co-expression of NK-1R (*green*), NK-3R (*red*), and choline acetyltransferase (ChAT, *blue*) in the GP. Note that ChAT expression was associated with strong NK-1R immunoreactivity, with faint NK-3R expression. The images of the immunofluorescence were captured with 10x (**a_1**) or 40x objective lens with the respective software (cellSens for BX-53, FLUOVIEW for FV1200, Olympus).

3.3. NK-1R-immunoreactive neurons occasionally expressed Lim-homeobox 6 (Lhx6) and parvalbumin (PV) but not forkhead box protein P2 (FoxP2)

Two types of NK-1R-immunoreactive neurons were observed in GP (Fig. 5a_2). The first type was large-sized strong NK-1R-immunoreactive neurons which have been already reported by previous studies. The other type was medium-sized and moderate immunoreactive NK-1R neurons (hereafter referred to as NK-1R neurons) I found. This new type of NK-1R neurons was homogeneously distributed in GP (Figs. 5a_1,11a). Hereafter, cell count values in the main text were derived from adult mice (7-12 postnatal weeks) unless otherwise noted, although I also showed data for young mice (21 postnatal days) in figures. I determined that the NK-1R neurons comprised of 38.9 ± 3.5% of all GP neurons determined by a neuronal marker, NeuN (Figs. 5b, 11b; N = 2,817 cells from 9 sections of 3 mice), and the proportion showed no significant difference along the LM axis (Fig. 11c, d). The second type of NK-1R neurons was composed of a large neuron with dense NK-1R staining throughout the soma to dendrites (Fig. 5a_2), which also expressed choline acetyltransferase (ChAT) (Fig. 10c). NK-1R and ChAT immunopositive neurons formed a very small proportion of all GP neurons (0.17 – 1.97%, estimated from maximum (5/254) and minimum (1/600) likelihood). In addition, it has been reported that ChAT expressing neurons in the GP had direct projection to frontal regions of the cortex and particular

firing properties (Saunders et al. 2014; Hernandez et al. 2015). Sine these features of ChAT expressing neurons are not common in the GP neurons, I excluded the strong NK-1R and ChAT immunopositive GP neurons from further analysis. See also technical consideration in "Discussion". For details on verification of the NK-1R antibodies, see "Materials and Methods" and Figs. 6-9, 12.

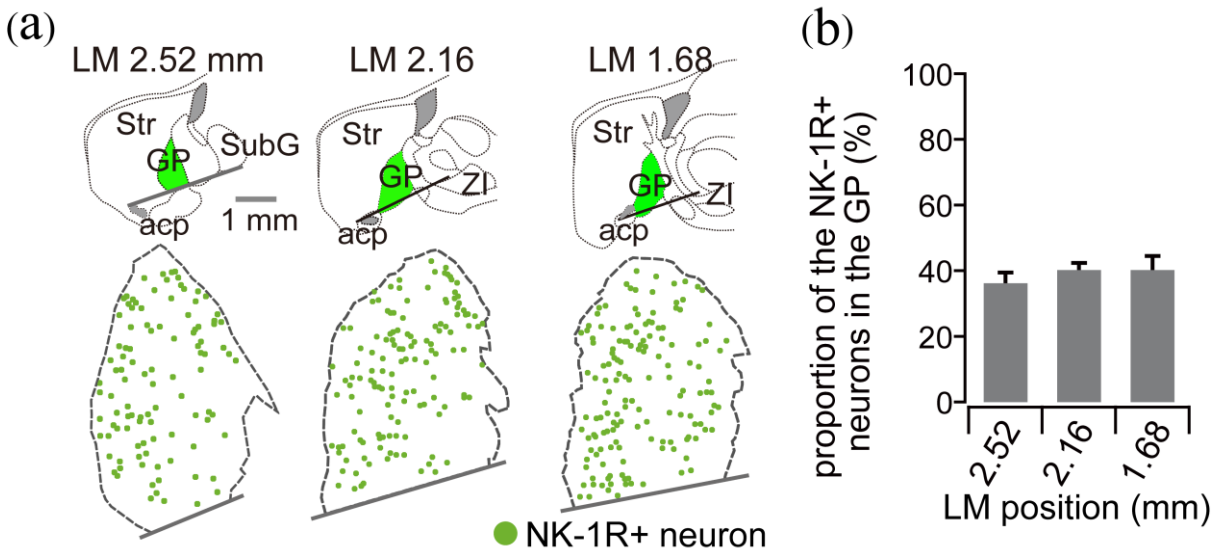

Figure 11. Distribution of the NK-1R neurons in the GP
a Distribution of NK-1R neurons in three lateromedial (LM) subdivisions of the GP. For GP neuron sampling in sagittal sections, the ventral borders of GP (*lines*) were defined according to the dorsal edge of the posterior limb of anterior commissure (acp) and the ventral edge of the subgeniculate nucleus of prethalamus (SubG, LM 2.52 mm), the dorsal edge of acp and the rostral edge of zona incerta (ZI, LM 2.16 mm) and the ventral edge of acp and the rostral edge of ZI (LM 1.68 mm), as shown in the upper panel. Only those neurons located dorsal to these borders were considered in the GP. **b** Frequencies of NK-1R expression in the GP. All GP neurons were detected with NeuN. Data were obtained across the lateral, central, and medial GP (N = 2,817 cells from 9 sections of 3 mice).

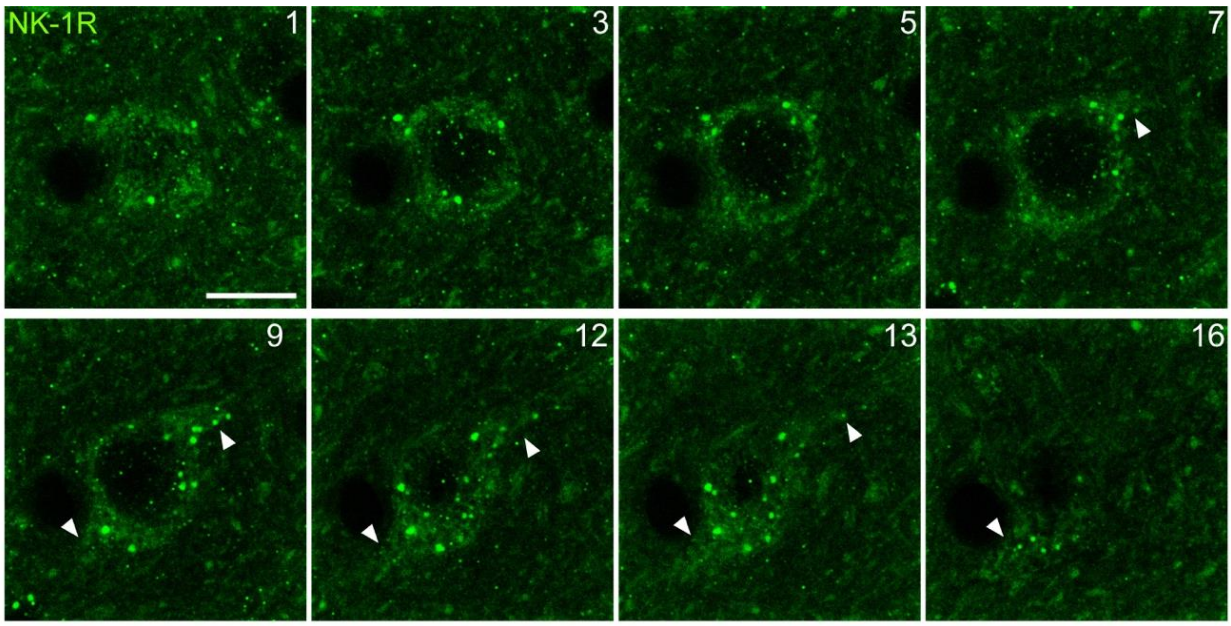

Figure 12. Confocal optic sections (0.35-μm step) of a single NK-1R immunoreactive neuron in GP.
Fluorescent signals were located close to membrane in a cell body and dendrites (*arrowheads*). Focal plane ID was shown at the upper right corner in each image. *Scale bar* 10μm.

To determine the localization of NK-1R in a neuron, I took images using the confocal microscopy for taking advantage of high Z-axis resolution. As a result, the signals were mostly distributed close to the membrane of a cell body (Fig. 12). Moreover, the membrane of proximal dendrites was also immunoreactive (*arrowheads* in Fig. 12).

Although the presence of the first type of NK-1R neurons in the GP was already reported in rats (Chen et al. 2009), their histochemical and projection characteristics were not well investigated in detail. Subthalamus (STN)-projecting cells, namely prototypic neurons, were known to express parvalbumin (PV) and/or Lim-homeobox 6 (Lhx6) (Mastro et al. 2014; Abdi et al. 2015; Dodson et al. 2015; Hernández et al. 2015). Given the continued debate regarding the proportion and molecular composition in the GP neurons (Flandin et al. 2010; Nóbrega-Pereira

et al. 2010; Mastro et al. 2014; Abdi et al. 2015; Dodson et al. 2015; Hernández et al. 2015), I used double or triple immunofluorescence to further determine whether NK-1R neurons might exhibit other molecular markers specific for GABAergic neuron subpopulations; the results of this evaluation are summarized in Fig. 13 and Fig. 14. In the present study on adult mice (7–12 weeks old; Fig. 13a, b, d, e for images; *gray bars* in Fig. 13c, f, g for quantification), 39.9 ± 3.6% and 52.8 ± 5.6% of GP neurons expressed PV (Fig. 13a, c; N = 6,850 cells from 18 sections of 3 mice) or Lhx6 (Fig. 13b, c; N = 3,653 cells from 9 sections of 3 mice), respectively. The proportion of GP neurons co-expressing both PV and Lhx6 was 21.1 ± 3.4% (Fig. 13 c_2; N = 916 cells from 3 sections of 1 mouse). I determined that 67.0 ± 7.5% and 82.2 ± 10.7% of NK-1R neurons co-expressed PV and Lhx6, respectively (N = 632 cells, from 9 sections of 3 mice; Figs. 13d, f). Neurons co-expressing both PV and Lhx6 often expressed NK-1R (81.4 ± 8.0%). Conversely, 59.1 ± 8.8% of NK-1R neurons co-expressed both PV and Lhx6. The co-expression of PV and forkhead box protein P2 (FoxP2) was negligible (FoxP2/PV = 0.1 ± 0.2%, N = 1,330 PV cells from 9 sections of 3 mice; PV/FoxP2 = 0.2 ± 0.3%, N = 926 FoxP2 cells from 9 sections of 3 mice; Figs. 14a, c). Among NK-1R neurons, only less FoxP2 immunoreactivity was observed (1.7 ± 2.5%; N = 567 NK-1R cells from 9 sections of 3 mice; Figs. 13e, f). Moreover, almost no FoxP2 neuron was immunoreactive for NK-1R (Figs 13e, g; 2.7 ± 3.9%; N = 309 FoxP2 cells from 9 sections of 3 mice). Multiple labeling for NK-1R and other neuronal markers in tissues taken from young/juvenile mice (21 days old, N = 2; *blank bars* in Fig. 13c, f, g) showed similar co-expression rate when compared with tissues taken from

adult mice. In addition, the similar result was obtained by another NK-1R antibody (Alomone Labs ATR-001; Fig. 13h, i). Therefore, I used juvenile mice for the following *in vitro* recording.

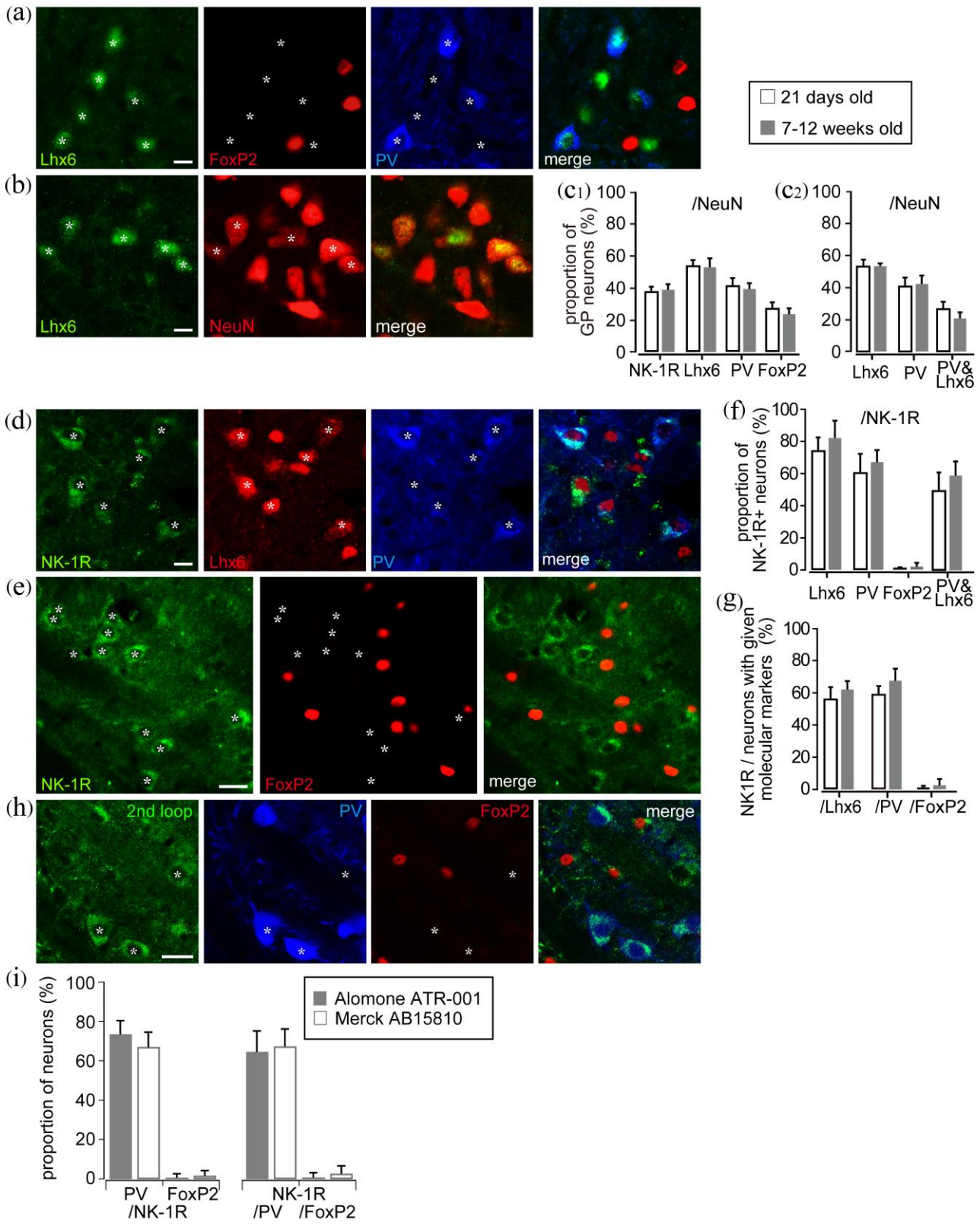

Figure 13. Co-expression profiles of NK-1R and other molecular markers in GP neuron classes of adult (7-12 weeks old) and young/juvenile (21 days old) mice. High-magnification images demonstrating the cellular expression of various GP neuron markers (**a**, **b**, **d**, **e**). **a** Lhx6 neurons (*green, asterisks*) frequently co-localized with PV (*blue*) but not with FoxP2 immunoreactivity (*red*). **b** Almost half of NeuN neurons (*red*) showed Lhx6 immunoreactivity (*green, asterisks*). **c** Expression frequencies of given molecular markers in all GP neurons, defined using the NeuN. **c_1** Pooled data across the lateral, central, and medial GP; 13,320 cells from 36 sections of 3 adult mice (7-12 weeks old) and 5,497 cells from 12 sections of 2 young/juvenile mice (21 days old). **c_2** Co-expression of Lhx6 and PV (N = 916 cells from 3 sections of one mouse). Data shown in **c_1** and **c_2** were derived from independent sample groups. **d** NK-1R neurons (*green, asterisks*) frequently co-localized with Lhx6 (*red*) and/or PV immunoreactivity (*blue*). **e** In contrast, almost no FoxP2 immunoreactivity (*red*) was observed in NK-1R neurons (*green, asterisks*). *Scale bars* in **a**, **b**, **d** 10 μm and in **e** 20 μm. **f** Expression frequencies of given molecular markers in NK-1R neurons. Data were pooled across the lateral, central, and medial GP; 1,198 cells from 18 sections of 3 adult mice (7-10 weeks old) and 1,550 cells from 12 sections of 2 young/juvenile mice (21 days old). **g** Expression frequencies of NK-1R in GP neurons with given molecular markers. Data were pooled across the lateral, central, and medial GP; 1,799 cells from 18 sections of 3 adult mice (7-10 weeks old) and 2,425 cells from 12 sections of 2 young/juvenile mice (21 days old). The photo-images were taken with an epifluorescent microscope (BX-53, Olympus, Tokyo, Japan) under the same conditions as described in the “Materials and Methods” section. **h** Triple immunofluorescent images for NK-1R (using Alomone ATR-001), parvalbumin (PV), and FoxP2. Note that NK-1R (*asterisks*) was frequently expressed in PV neurons, not in FoxP2 neurons. **i** Co-expression properties of NK-1R by Merck AB15810 (*blank bars*) and Alomone ATR-001 (*gray bars*) with PV or FoxP2. Data ware sampled from 12 regions of interest in 2 sections. By the Alomone antibody, 73.5 ± 7.0% of NK-1R immunoreactive neurons co-expressed PV, whereas only 0.7 ± 2.0% of NK-1R immunoreactive neurons co-expressed FoxP2. Conversely, NK-1R was expressed in 67.4 ± 8.8% of all PV immunoreactive neurons, and only in 0.8 ± 2.4% of all FoxP2 immunoreactive neurons (*right, gray bars*, N = 327 cells in 3 sections from one mouse). These co-expression profiles investigated with Alomone ATR-001 were very similar to those obtained by the Merck AB15810.

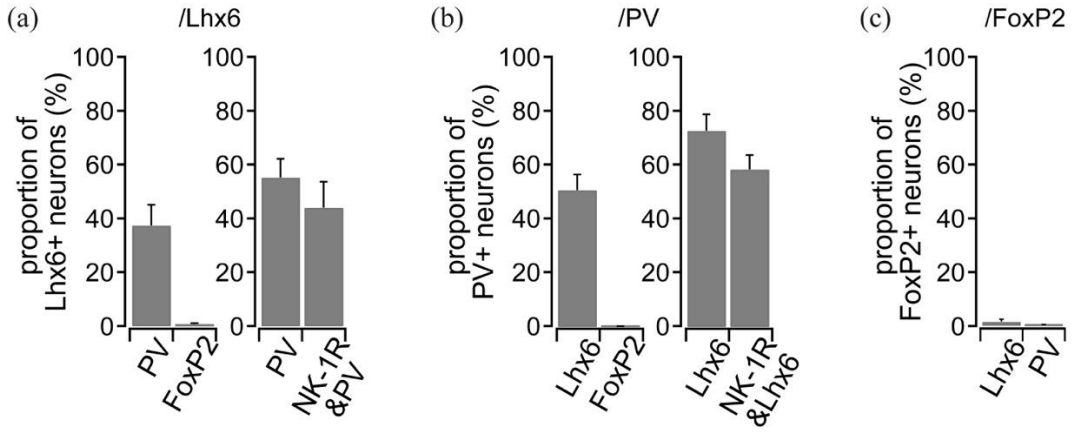

Figure 14. Co-expression profiles of Lhx6, PV, NK-1R and FoxP2 in GP neuron classes of adult mice (7-10 weeks old).
a *Left*, Lhx6 neurons frequently co-expressed PV (37.4 ± 7.7%) but not FoxP2 (0.8 ± 0.3%). *Right*, Lhx6 neurons co-expressed PV (55.2 ± 9.6%) or both PV and NK-1R (44.1 ± 6.9%). Data for *Left* and *Right* were obtained from different data samples (N = 9 sections of 3 mice for each). **b** *Left*, The half of PV neurons co-expressed Lhx6 (50.8 ± 5.8%), whereas FoxP2 was not expressed in PV neurons (0.1 ± 0.2%). *Right*, Lhx6 (72.9 ± 6.1%), or both Lhx6 and NK-1R (58.5 ± 5.3%) were frequently observed in PV neurons. Data for *Left* and *Right* were derived from different data samples (N = 9 sections of 3 mice for each). **c** In contrast, FoxP2 neurons co-expressed neither PV (0.2 ± 0.3 %) nor Lhx6 (1.6 ± 0.8%). Data were derived from 9 sections (3 mice). In total, 5,650 cells from 18 sections of 7 mice were counted.

3.4. NK-1R neurons are subgroup of prototypic neurons but not arkypallidal neurons

As demonstrated above, our findings of co-expression of NK-1R and PV/Lhx6 raised a hypothesis that NK-1R could be expressed exclusively in prototypic GP neurons. I examined this possibility by direct observation of NK-1R expression in prototypic or arkypallidal neurons by a combination of immunofluorescence and injection of retrograde tracer into the STN (Fig. 15d) or striatum (Fig. 16b), respectively.

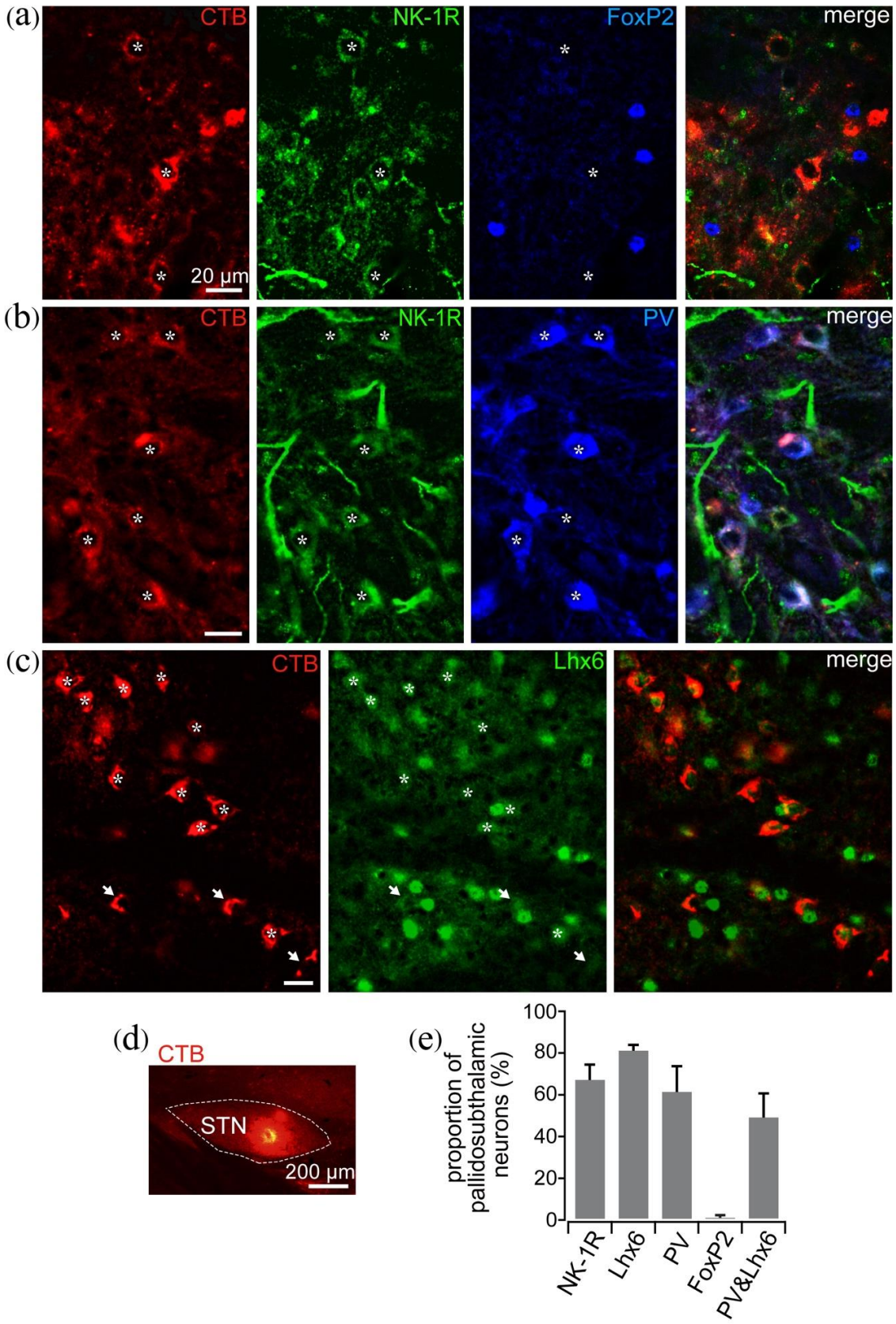

Figure 15. Preferential expression of NK-1R in pallidosubthalamic neurons.

a Pallidosubthalamic neurons identified by retrograde labeling with Alexa Fluor 555-conjugated cholera toxin subunit B (CTB) (*red, asterisks*) frequently possessed NK-1R (*green*) but not FoxP2 (*blue*). **b** CTB neurons frequently showed NK-1R (*green*) and/or

PV immunoreactivity (*blue*). **c** The majority of CTB neurons (*red*) showed Lhx6 immunoreactivity (*green, asterisks*), but some CTB neurons showed no Lhx6 immunoreactivity (*arrows*). **d** Verification of a site of CTB injection into the subthalamic nucleus (STN). **e** Proportions of neurons expressing the given molecular markers in pallidosubthalamic neurons, defined with CTB labeling (data were pooled across the lateral, central, and medial GP; 749 cells from 9 sections of 3 mice). See also Fig. 3.

As a result, 67.1 ± 7.3% (N = 221 cells from 9 sections of 3 mice) of STN-projecting cells showed NK-1R immunoreactivity (Fig. 15a, b, e), whereas almost none of STN-projecting cells showed FoxP2 immunoreactivity (0.34 ± 1.0%; N = 232 cells from 9 sections of 3 mice, Fig. 15a, b, e); this is consistent with other previous reports (Dodson et al. 2015; Hernández et al. 2015). It should be noted that molecular expression of STN-projecting neurons was a bit different from previous reports: PV was expressed in 61.4 ± 12.3% of STN-projecting neurons, Lhx6 was in 81.1 ± 2.8% (Fig. 13c, e), and both PV and Lhx6 were in 49.0 ± 11.6 % (cf. Abdi et al. 2015; Hernández et al. 2015). On the other hand, striatum-projecting cells putatively contained both arkypallidal and prototypic neurons, since prototypic neurons also possess striatal collaterals (Mallet et al. 2012; Fujiyama et al. 2015). They were also distributed throughout the GP. I confirmed that 41.7 ± 16.0% (N = 361 cells from 9 sections of 2 mice) of pallidostriatal neurons were arkypallidal which expressed FoxP2 (Fig. 16a, c, e, f) with almost no co-expression of NK-1R (0.6 ± 1.7%; N = 149 FoxP2-expressing pallidostriatal cells from 9 sections of 2 mice). However, only a few expressions of PV (9.3 ± 5.1%, N = 361 cells from 9 sections of 2 mice) and no co-expression of PV and FoxP2 were observed. Contrarily, other 25.9 ± 10.6% (N = 663 cells from 18 sections of 2 mice) of pallidostriatal neurons were NK-1R-immunopositive, which frequently possessed Lhx6 (75.3 ± 16.0%; N = 86 cells from 9 sections

of 2 mice, see Fig. 16d, g) but rarely possessed PV immunoreactivity (16.1 ± 12.3%; N = 172 cells from 18 sections of 2 mice, see Fig. 16d, e). These neurons could be considered as prototypic neurons possessing pallidostriatal collaterals. All these results suggested NK-1R neurons compose a specific subpopulation of GP prototypic neurons. Since electrophysiological properties of different molecular types of GP neurons also differed from each other (Abdi et al. 2015; Hernández et al. 2015), I hypothesized that SP-responsive neurons could also be differentiated electrophysiologically.

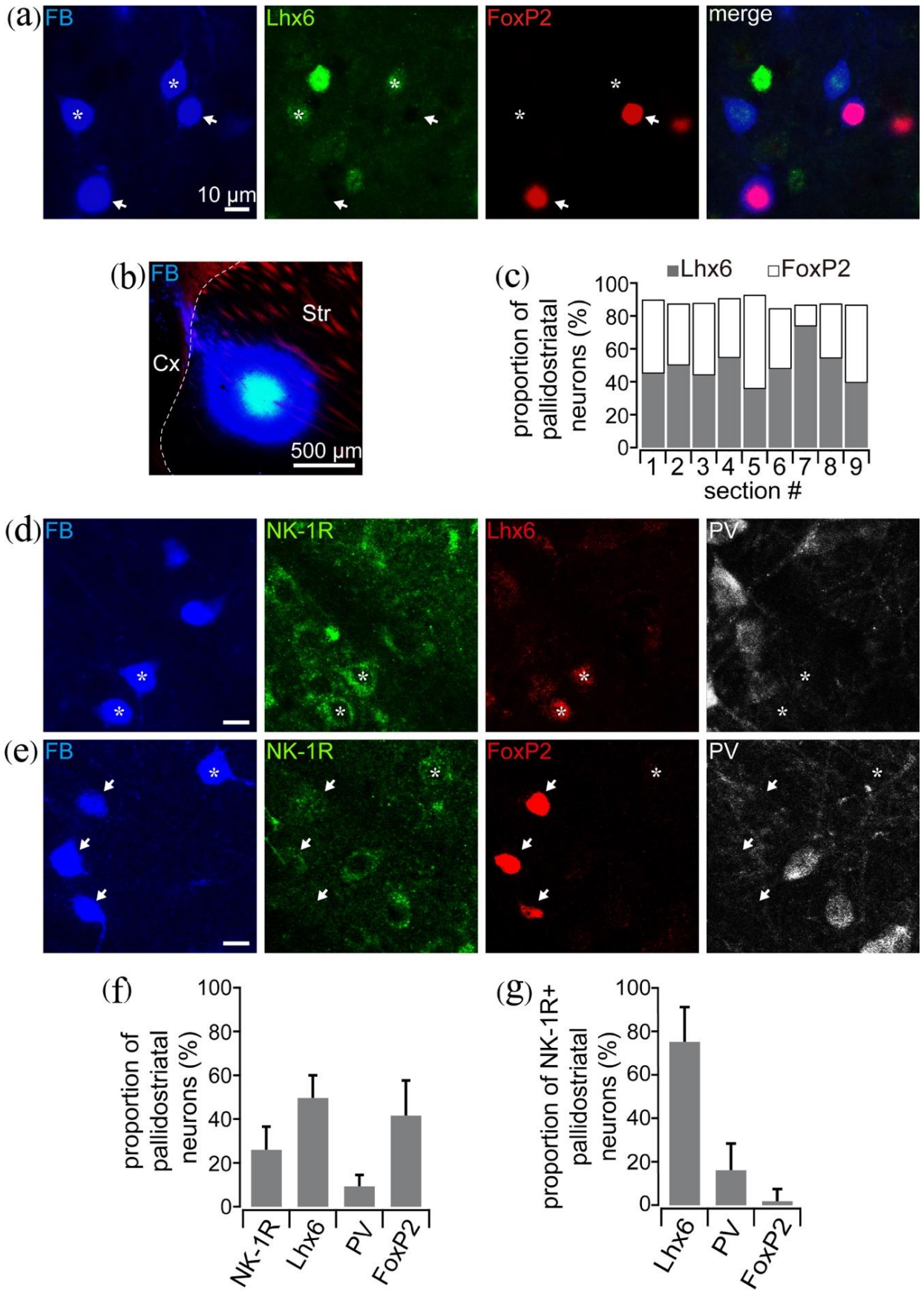

Figure 16. Expression of NK-1R in Lhx6-positive pallidostriatal neurons but not in FoxP2-positive arkypallidal neurons.

a Pallidostriatal neurons identified by retrograde labeling using Fast Blue (FB, *blue*) exclusively co-localized with Lhx6 (*green, asterisks*) or FoxP2 immunoreactivity (*red,*

arrows). Note that no Lhx6 neurons (*green*) co-localized with FoxP2 immunoreactivity (*red*).
b Verification of a site of FB injection into the striatum (Str). *Cx* cerebral cortex. **c** Proportions of neurons expressing Lhx6 and FoxP2 immunoreactivity in pallidostriatal neurons (data were pooled across the lateral, central, and medial GP; 352 cells from 9 sections of 2 mice). Note that almost all pallidostriatal neurons showed either Lhx6 or FoxP2 immunoreactivity. **d** FB neurons (*blue*) showing NK-1R immunoreactivity (*green, asterisks*) highly co-localized with Lhx6 (*red*) but not with PV immunoreactivity (*gray*). **e** FB neurons (*blue*) with FoxP2 immunoreactivity (*red, arrows*) showed neither NK-1R (*green*) nor PV immunoreactivity (*gray*). Note that one FB neuron with NK-1R immunoreactivity (*asterisk*) showed neither FoxP2 nor PV immunoreactivity. **f** Proportions of neurons expressing the given molecular markers in pallidostriatal neurons (data were pooled across the lateral, central, and medial GP; 1,326 cells from 36 sections of 2 mice). **g** Proportions of the given molecular markers expressing neurons in NK-1R immunopositive pallidostriatal neurons (data were pooled across the lateral, central, and medial GP; 232 cells from 27 sections of 2 mice). *Scale bars* in **d** and **e** were 10 μm.

3.5. Effect of SP onto GP neurons

I conducted *in vitro* whole cell recordings from GP neurons to investigate how SP affects them and what type of GP neurons responds. SP receptor agonist, [Sar^9, $Met(O_2)^{11}$]-SP (SM-SP), which is potent and selective for NK-1R, was applied to the recorded neurons through another glass pipette containing 0.1 or 1 mM of SM-SP using a brief air pulse (5–10 psi for 10–100 ms; Fig. 17a). Among the 48 GP neurons examined (N = 31 mice; P17–27), SM-SP induced prolonged inward current in 21 neurons at around mean membrane potential in voltage clamp mode (Fig. $17a_1$, *top*) or action potentials in current clamp mode (Fig. $17a_2$). The remaining 27 GP neurons did not respond to SM-SP puffs (Fig. $17a_1$, *bottom*). The inward current was not inhibited by bath application of glutamate and $GABA_A$ receptor antagonists (CNQX, 10 μM; D-AP5, 20 μM; SR95331, 20 μM; N = 7; Fig. 17b, c). Moreover, additional bath application of NK-1R antagonist, SR140333, prevented SM-SP-induced current (N = 2 cells; Fig. 17c). It

could be possible that long duration of recording deteriorates the response irrespective of the presence of SP receptor antagonist; however, it would not be the case. For control experiments without SP receptor antagonist, I recorded neurons for long duration (<90 min) and confirmed the response against SM-SP puffs still remained (Fig. 18). For another control experiment, I applied an ACSF puff against two cells which responded the SM-SP puff (N = 2 cells), and found that no response was elicited (data not shown). Taken together, the SM-SP puff response observed here was likely to be actually elicited by SM-SP, although the fast onset and offset were atypical via metabotropic receptors. The SM-SP induced response was dependent on holding potential on both amplitude and prolonged duration, and increased with depolarization (N = 5 cells; Fig. 17e). For comparison, the peak amplitude (Fig. 17f_1) and the calculated charge (Fig. 17f_2) were normalized to the maximum response of each neuron. The peak amplitude of SM-SP-induced current reached the maximum around –40 mV (Fig. 17f_1); however, beyond this range, an action current was induced by SM-SP puffs that masked the SM-SP-induced current itself. In contrast, the SM-SP-induced current decreased with hyperpolarization, although it was still observed as an inward current at –70 mV. Thus, equilibrium potential would be a more hyperpolarized range as already reported (Chen et al. 2009). The charge was also correlated with the holding potential and became larger by depolarization, however, in some cases, depolarization beyond –40 mV decreased the charge. This would be likely due to shortening of SM-SP-induced inward current duration in some cases. Moreover, two SM-SP-responded neurons were morphologically recovered, and those

were found as immunopositive for NK-1R (Fig. 17d; N = 2/2). Together with the above-mentioned morphological data (Figs. 14, 15, 16), SM-SP-responsive neurons may be restricted in a subpopulation, around half of GP neurons. Next, I analyzed electrophysiological properties of GP neurons in detail to further characterize NK-1R neurons.

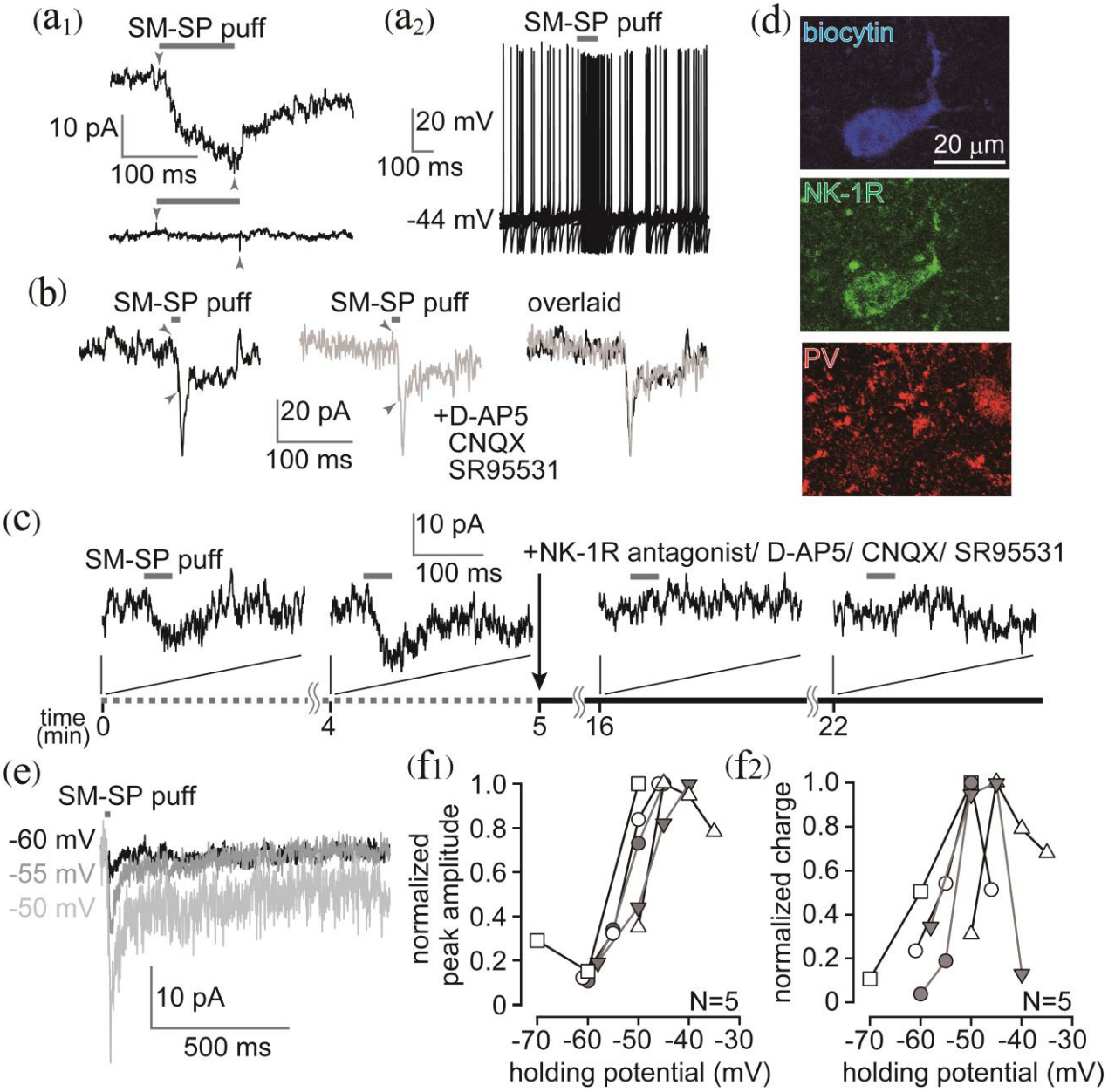

Figure 17. SP agonist (SM-SP) induced action potentials or inward current.
a SM-SP puff stimulation induced excitation in a subset of GP neurons. **a₁** *Upper* a GP neuron responded to the application of 1 mM SM-SP (a 100-ms puff, *gray bar*). *Bottom*, a GP neuron that did not respond to the SM-SP (1 mM for 110 ms). The holding potential was set at –50 mV for both neurons. The traces were an average of ten

repetitive sweeps. In total, 21/48 GP neurons responded to an SM-SP puff stimulus. *Gray arrowhead* showed stimulus artifact at the onset and offset of an air puff. **a_2** In the current clamp mode, SM-SP elicited action potentials. The overlay of ten sweeps was represented. No DC current was applied. **b** SM-SP-induced current was not inhibited by antagonists for glutamate (D-AP5 20 μM; CNQX 10 μM) and $GABA_A$ (SR95531 20 μM) receptors. *Right*, overlay of the two traces. **c** The SM-SP-induced current was prevented by bath application of NK-1R antagonist, SR140333 (10 μM). In this neuron, an SM-SP puff at 0 and 4 min, without NK-1R antagonist, induced inward current at -50mV of holding potential, whereas 11 and 16 min after NK-1R antagonist application (shown as *black line*), the effect of SM-SP puff diminished. **d** An example of recorded neuron visualized with biocytin (*blue*). Using immunofluorescence combined with tissue cleaning (AbScale), the presence of NK-1R in the recorded neuron was revealed (*green*). The neuron also showed faint PV immunoreactivity (*red*), which was much weaker than that of a non-recorded neuron located in the right side of the recorded neuron, probably due to long recording. **e** Voltage dependence of SM-SP-induced currents. The holding potentials are shown at left. Each trace was the average of ten sweeps. **f** Normalized amplitude of SP induced peak current **f_1** or charge **f_2** was plotted against holding potential (N = 5 cells). SM-SP-induced currents were larger at more depolarized holding potential. Note that the polarity of the current was not reversed even at –70 mV. SM-SP-induced charge was calculated over 1-second period after the SM-SP puff paused, to capture the prolonged effect. The charge was also smaller in hyperpolarized membrane potential, although, it tended to decrease by depolarization beyond –40 mV.

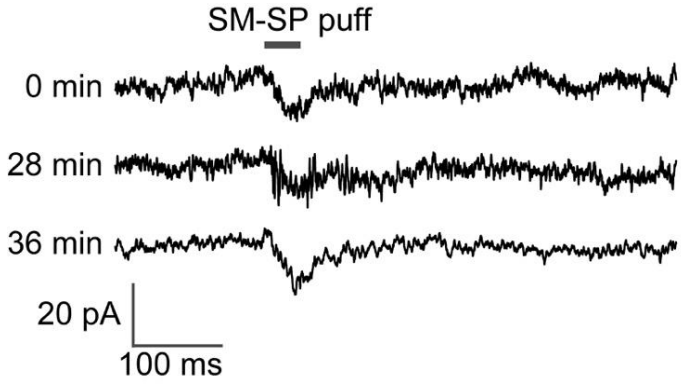

Figure 18. SM-SP induced inward current during long duration of recording.

3.6. Electrophysiological properties of GP neurons and their correlation with SM-SP response

Basic membrane responses were recorded using current pulse steps in 92 GP neurons, before the application of SM-SP or other drugs (N = 31 mice, P15–27; including the above-mentioned 48 neurons). I analyzed the membrane input resistance (R_{in}), time constant (tau), and hyperpolarizing sag potential (sag), and found those properties were similar to those reported earlier (Table 3; cf. Cooper and Stanford 2000; Mastro et al. 2014; Abdi et al. 2015; Hernández et al. 2015). On the other hand, some properties were relatively different comparative to the reports. For example, spontaneous firing was observed only in 64 cells (0.2–69.4 Hz, on average 11.4 Hz; Fig. 19a). The proportion of active cells was similar to the result of Cooper and Stanford (2000), however, much smaller than the results of other groups. This discrepancy could be caused by the fact that our recordings were obtained using conventional whole cell recording, not perforated patch method. Thus, spontaneous activity reported here may not reflect behaviors of intact neurons. In addition, while recording the activity, bath solution did not contain any pharmacological reagents, thus it was not purely autonomous activity. With regard to firing properties during depolarizing pulses, at least two distinct types of GP neurons were qualitatively observed (Fig. 19b, c). One type (Fig. 19 *left column*) possessed a narrow action potential with fast after hyperpolarization (fAHP; *arrowhead* in Fig. 19a_1, d_1). Occasionally they lacked slow AHP (sAHP; Fig. 20f, *inset*, Table 3).

Table 3. Electrophysiological properties of the three clusters of GP neurons

	cluster 1	cluster 2	cluster 3	*p* value
total number of cells	24	32	36	
mean membrane potential (mV)	–54.4 ±11.0 (–40.1 to –77.2)	–53. 1 ± 6.1 (–44.3 to –70.0)	–50.5 ± 5.7 (–41.9 to –66.6)	0.11
input resistance (MΩ)	372.0 ± 242.5 (91.8 – 843.2)	256.5 ± 142.9* (51. 8 – 568.5)	339.6 ±135.4 (57.5 – 660.4)	0.03 (CL1-2, 0.039)
time constant (ms)	13.6 ± 6.6 (5.0 – 31.0)	10.9 ± 6.0 (2.3 – 25.9)	15.0 ± 5.7 (4.6 – 29.2)	0.10
spike height (mV)	75.46 ± 11.2 (49.5 – 91.5)	78.7 ± 7.0** (63.0 – 94.8)	70.1 ± 8.9 (54.7 – 89.4)	0.0003 (CL2-3, $<10^{-3}$)
spike width (ms)	1.87 ± 0.36 (1.23 – 3.93)	0.91 ± 0.16 (0.68 – 1.41)	1.20 ± 0.36 (0.68 – 2.17)	$< 10^{-10}$ a
spike threshold (mV)	–32.8 ± 4.2 (–40.2 to –23.4)	–42.0 ± 2.6 (–48.1 to –39.8)	–35.8 ± 2.4 (–40.4 to –30.6)	$< 10^{-15}$ a
spike counts by a 100 pA pulse (/s)	14 ± 14 (1 – 48)	29 ± 19 (0 – 69)	47 ± 26 (0 – 117)	$< 10^{-7}$ a
maximum spike counts (/s)	24 ± 24 (2 – 76)	148 ± 39 (82 – 229)	116 ± 54 (51 – 286)	$< 10^{-16}$ a
fAHP amplitude (mV)	–24.9 ± 6.6 (–36.9 to –12.7)	–23.5 ± 3.4 (–32.2 to –15.7)	–23.7 ± 5.2 (–33.1 to –14.3)	0.25
fAHP delay (ms)	2.3 ± 0.6** (1.7 – 3.7)	1.0 ± 0.2 (0.7 – 1.7)	1.5 ± 0.6 (0.7 – 3.8)	< 0.002 (CL1-2,1-3, $<10^{-4}$)
number of neurons with sAHP**	20/24**	10/32	15/36	CL1-2, $<10^{-3}$; CL1-CL3, 0.007
sAHP amplitude (mV)	–31.0 ± 9.7** (–52.4 to –20.0)	–21.0 ± 4.7 (–27.6 to –11.8)	–21.8 ± 2.8 (–26.5 to –16.8)	0.003 (CL1-2, 0.001; CL1-3, 0.001)
sAHP delay (ms)	22.1 ± 10.5* (4.0 – 44.7)	15.7 ± 8.7 (4.2 – 30.5)	13.9 ± 4.6 (5.8 – 23.1)	0.008 (CL1-2, 0.022; CL1-3, 0.008)
sag potential (mV)	9.5 ± 9.1 (0.3 – 30.9)	9.2 ± 6.1* (1.1 – 23.0)	13.6 ± 8.0 (0.9 – 34.0)	0.03 (CL2-3, 0.049)
number of neurons with spontaneous firing	13/24	20/32	28/36	0.13
spontaneous firing frequency (Hz)	2.2 ± 0.6* (1.5 – 3.7)	11.6 ± 14.8 (1.2 – 69.4)	15.6 ± 12.3 (0.6 – 53.9)	0.0001 (CL1-3, 0.02)

Data are presented as mean ± SD. The minimum and maximum values of each parameter are shown in the parenthesis. For sAHP and spontaneous firing frequency, neurons lacking sAHP or spontaneous firing were omitted from calculation. Statistical

significance was examined by one-way ANOVA followed by post hoc Tukey test (* p < 0.05; ** p <0.01). p values for ANOVA are presented in the far right side of the columns and those for Tukey test were in the parenthesis. Difference of proportion of neurons with sAHP or spontaneous firing was tested by pairwise comparison with Holm's p value correction. [a] See Fig. 20 for details.

One second of depolarizing current pulses evoked those fast and non-accommodated repetitive firing. Firing frequency linearly increased along with the strengthening of current intensity and reached the maximum frequency beyond 100 Hz (Fig. 19b_1, c_1). Occasionally, a large sag potential was observed against a hyperpolarizing current pulse (Fig. 19e_1 *arrowhead*). Contrarily, another type of GP neurons was characterized by a relatively wide action potential and low firing frequency even when a higher current was applied (Fig. 19, *right column*). Most of them possessed sAHP in addition to fAHP. Fifty-six neurons became quasi-silent by high-intensity current injection, which was so-called depolarizing block. Major GP neurons including these two types showed relatively small rheobase (Fig. 19f, g).

Since, it was not possible to classify the GP neurons clearly using one electrophysiological feature because the electrophysiological features of GP neurons continuously varies, I performed the multiple classification analysis to investigate the electrophysiological properties of SM-SP responded neurons. To objectively distinguish these GP neuron types, cluster analysis was applied by Ward method using four electrophysiological parameters: spike width, spike frequency at 100 pA depolarization, the maximum spike frequency, and action potential threshold in collaboration with Dr. Fuyuki Karube. It should be mentioned that action potential threshold was a bit depolarized in our recordings, compared to the earlier reports (Cooper and

Stanford 2000; Mastro et al. 2014; Abdi et al. 2015; Hernández et al. 2015). It might come from the difference of recording conditions and definition of action potential threshold (see "Materials and Methods"). As shown in Fig. 20a, two large clusters were segregated. The first cluster (CL1) was composed of 24 neurons possessing a broad spike and low firing frequency (Fig. 19, *right column*). The other cluster could be further divided into two sub clusters, referred to as CL2 (N = 32 cells) and CL3 (N = 36 cells). One-way ANOVA revealed the four parameters used for the cluster analysis were significantly different among the neurons in these three clusters ($p < 10^{-7}$).

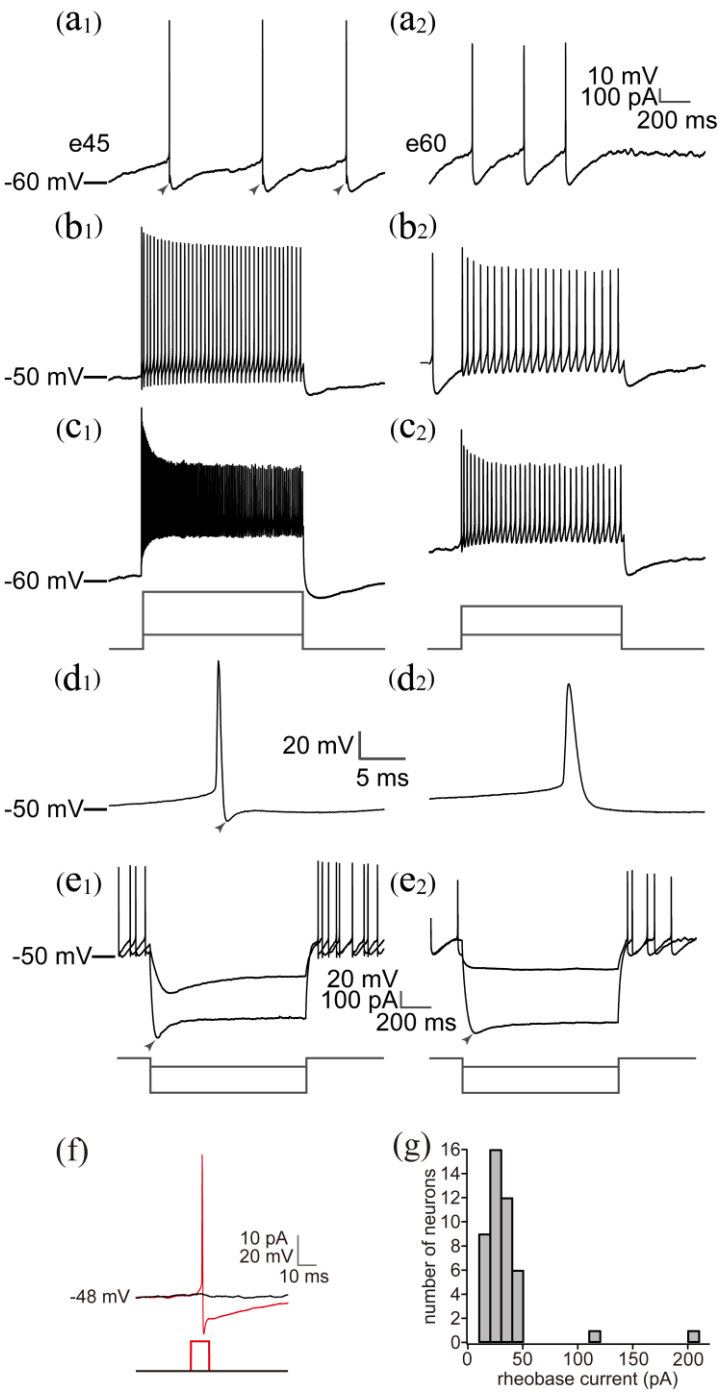

Figure 19. Two representative electrophysiological types of GP neurons.

a-e Each *column* represents one typical neuron, neuron 1 (*left*) and 2 (*right*). **a** Spontaneous firing. Note **a₁** spikes possessed fast after hyperpolarization (fAHP, *arrowheads*). **b** Firing response against a 1 s of 100 pA depolarizing pulse. Faster and non-accommodating firing response was observed in **b₁**. **c** Firing with maximum frequency elicited by 1 s of depolarizing pulse. Current intensity was 400 pA for **c₁** and 300 pA for **c₂**. Again, **c₁** showed faster firing. **d** Magnified view of an action potential. Note the narrow width and fAHP (*arrowhead*) for **d₁** and the relatively wide action potential lacking fAHP for **d₂**. **e** Responses against hyperpolarizing pulses (–50 and –200 pA). Sag potential was observed for both cells (*arrowheads*). *Scale* in **a** was also applied to **b** and **c**. **f and g** Rheobase current of GP neurons. **f** Rheobase current was

measured by 10 ms-current pulse steps application. Current intensity was increased by 10 pA. The rheobase of this neuron was 10 pA. **g** Frequency distribution of rheobase in 45 GP neurons. Except for 2 neurons, an action potential was elicited by <50 pA current, indicating high excitability of GP neurons.

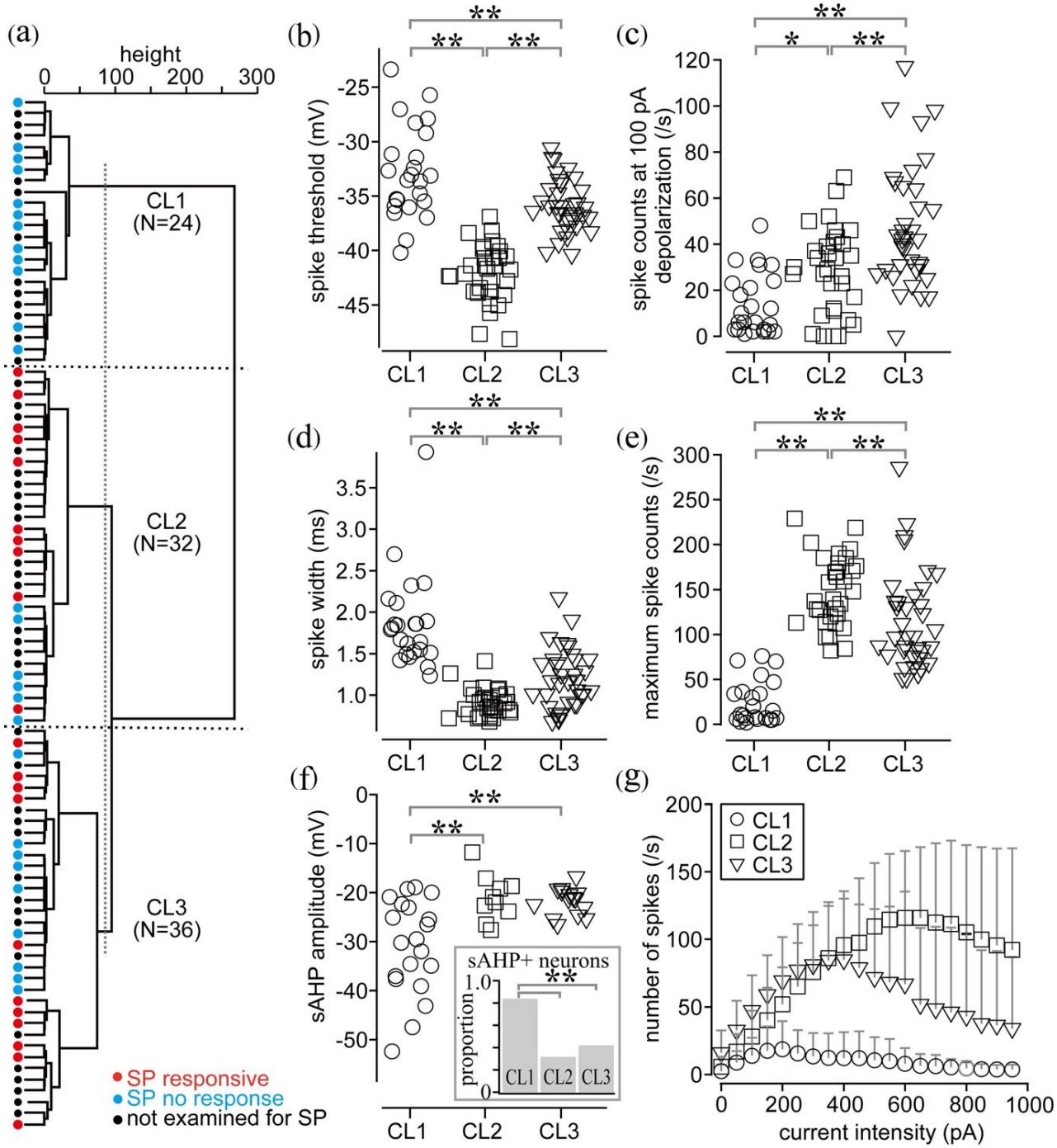

Figure 20. The cluster analysis identified three electrophysiological types involved in SM-SP response.

a The cluster analysis (Ward method) divided 92 GP neurons into three clusters, CL1, CL2, and CL3. Electrophysiological parameters used for the analysis are shown and compared in **b**–**e**. Note that SM-SP-responsive neurons were exclusively observed in CL2 and CL3, not in CL1. **b**–**e** Comparison of electrophysiological parameters among

three clusters. Statistical significance was examined by one-way ANOVA followed by post hoc Tukey test (* $p < 0.05$; ** $p < 0.01$). **b** Spike threshold was more depolarized in CL1 and CL3 than CL2, and in CL1 than CL3. **c** Number of spikes elicited by a 1 s of 100 pA pulse. CL1 neurons fired less number of spikes than others. **d** Spike full width at the level of the spike threshold. CL1 spikes were broader than others. **e** Maximum spike frequency by 1-s depolarizing pulse. Note that the current intensity, which induced the maximum number of spikes, differed among neurons (range 200–950 pA). CL2 could fire more numerous spikes than others, and CL3 could fire more numerous spikes than CL1. **f** sAHP amplitude was larger in CL1 than others. Inset shows proportion of neurons possessing sAHP. CL1 contained larger proportion of neurons with sAHP than others. **g** Relationship of firing frequency and injected current intensity. Depolarized pulses were applied by 50 pA steps from 50 to 950 pA. CL1 follows higher current intensity with fast firing, whereas CL1 reached the maximum frequency by a small current intensity. One-way ANOVA revealed significant differences among clusters at all current steps ($p < 0.001$). Post hoc Tukey test confirmed CL1 and CL2 differed from each other above 150 pA ($p < 0.01$). CL1 and CL3 differed from each other at the current range of 0–700 pA ($p < 0.01$). Significant differences between CL2 and CL3 appeared below 100 pA and over 500 pA ($p < 0.01$).

Table 4. *p* value for multiple comparisons

comparison	spike width	spike threshold	spike frequency at 100 pA depolarization	maximum spike frequency
CL1 vs CL2	$< 10^{-7}$	$< 10^{-7}$	0.0359	$< 10^{-7}$
CL1 vs CL3	$< 10^{-7}$	0.0010	10^{-7}	$< 10^{-7}$
CL2 vs CL3	0.0058	$< 10^{-7}$	0.0012	0.0066

Further multiple comparisons for the parameters were examined by post hoc Tukey test, which confirmed the significance of the differences (Fig. 20b-e; Tables 3, 4). Other parameters, which were not used for the cluster analysis, were also examined in the same way. As a result, the parameters on the AHP and sag potential differed among three clusters (Fig. 20f; Table 3). Most of the CL1 neurons, 20/24, possessed sAHP which is defined here as AHP that reached the negative voltage peak longer than 4 ms after the spike peak with a slower depolarizing phase. On the contrary, sAHP was less frequently observed in CL2 (10/32) and CL3 (15/36)

neurons (Fig. 20f). The proportion of neurons with sAHP was significantly larger in CL1 ($p <$ 0.007). The sAHP of CL1 was larger in amplitude ($p = 0.001$) than others and slower than others ($p < 0.022$). The relationship between injected current intensity and spike frequency also differed among clusters (Fig. 20g). CL1 was composed of neurons with strong accommodation; indeed, their spikes could follow the increment of current intensity only up to ~250 pA, and beyond the range, spike frequency did not increase. However, many of them did not become silent even when higher intensity of current was injected. CL2 neurons could linearly respond to increasing of current intensity until ~800 pA, resulting in the highest firing frequency among the three clusters. CL3 showed the moderate properties. Within the range of current intensity less than 450 pA, CL3 firing was similar with that of CL2, however, they reached the maximum spike frequency at ~400 pA. The above spike frequency-current intensity curves differed significantly among clusters ($p < 0.01$ in current ranges > 500 pA or < 100 pA by one-way ANOVA). Multiple comparisons revealed that the difference between CL1 and CL2 became significant at 150 pA and further ($p < 0.01$). For CL1 and CL3, significant differences were observed from 0 to 850 pA ($p < 0.05$; $p < 0.01$ at current intensity < 700 pA). It is likely that this difference partially reflected the ratio of depolarizing block, because 13 of 32 CL2 neurons showed depolarizing block, whereas 30 of 36 CL3 neurons did. In addition, spontaneous firing was investigated for only 5 s, soon after cells were in a whole cell mode. The reason why the short duration was to avoid gradual changes of intracellular conditions, because, again, I did not employ perforated patch clamp method. Thus attention must be paid

that spontaneous activity reported here could not be the same as that of intact neurons. Even with such a limitation, spontaneous firing was more frequently observed in CL2 and CL3 than in CL1, although the frequency of spontaneous firing was significantly different only between CL1 and CL3 (Table 3). Interestingly, I found a clear relationship between SM-SP response and clusters. All SM-SP-responsive neurons were in CL2 (10 responsive neurons/ 16 neurons examined) and CL3 (11/20), and were completely absent in CL1 (0/12).

4. Discussion

In summary, I found new type of NK-1R expressing GP neurons which showed moderate immunoreactivity to the NK-1R. This type of neurons was classified into prototypic type neurons by molecular expression, projection pattern and electrophysiological properties. I also showed almost no NK-1R expression in another type of GP neurons, arkypallidal neurons. I will discuss below significance of highly cell type specific expression of NK-1R in GP.

In this thesis I examined the properties of the NK-1R neurons in the GP and clarified the following points. 1) NK-1R neurons occasionally expressed Lhx6 and PV but not FoxP2. 2) NK-1R neurons were classified as a subgroup of the prototypic GP neurons by immunofluorescence and projection pattern. 3) SP agonist induced firing or inward current to a part of GP neurons and this effect was inhibited by the SP antagonist specifically. 4) SP agonist-responsive neurons were identified as the prototypic GP neurons by the cluster analysis. Thus, I found cell type-specific expression of NK-1R in the mouse GP based on morphological and electrophysiological experiments. First of all, I argued reliability of our present results with respect to potential methodological concerns.

4.1. Technical Considerations

In the present study, two types of NK-1R neurons were observed in GP. One type was composed of a large neuron with dense NK-1R staining throughout the soma to dendrites,

which also expressed ChAT (Fig. 10). This type of NK-1R neurons is well established by immunohistochemistry (Nakaya et al. 1994) and *in situ* hybridization studies (Elde et al. 1990; Gerfen 1991). Both of immunofluorescence and *in situ* hybridization in the present study also showed the outstanding signals of this type of NK-1R neurons (Fig. 5a and Figs. 6-9, 12 for immunofluorescence, Fig. 9 for *in situ* hybridization). Another type of NK-1R neurons was homogeneously distributed in GP throughout the LM axis (Fig. 11). Although autoradiographic technique revealed that a moderate level of NK-1R was expressed in GP in rat (Quirion et al. 1983; Mantyh et al. 1984), only two groups, as far as I know, reported that a moderate number of weak-positive NK-1R neuron was observed in GP in rat (Lévesque et al. 2003; Chen et al. 2009) and human (Mounir and Parent 2002). To further confirm the existence of these NK-1R neurons, I additionally examined other two different antibodies against the C-terminus (Table 1, Fig. 6), as well as one antibody against the second extracellular loop of the NK-1R peptide (Figs. 7, 8 Table 1). Immunofluorescence with those four antibodies resulted in similar images in central nervous system, including the striatum, ventral pallidum, nucleus basalis, and GP. In addition, GP contained two types of NK-1R neurons: a small population of strong immunopositive NK-1R neurons co-expressing ChAT (Fig. 10) and larger population of moderate immunopositive NK-1R neurons co-expressing PV or Lhx6 (Fig. 13). Furthermore, these NK-1R neurons showed no FoxP2 immunoreactivity with any of the antibodies (Figs. 7, 13, 14). The synthetic peptide (385-407), corresponding to the antigen of Merck AB15810 antibody, showed no homology with

other receptors, including NK-2R or NK-3R (NCBI Blast: https://blast.ncbi.nlm.nih.gov/Blast.cgi?PAGE_TYPE=BlastSearch). Even for whole sequences, the homology of NK-1R and NK-3R was under 50%, and the homologous site is not C-terminus of NK-1R, which is the immunogen of NK-1R antibodies. Altogether, the above supported that our present observation on moderate expression of NK-1R in GP neurons was not an artifact or cross reaction with other proteins, although I could not reveal mRNA expression (Fig. 9). It is possible that immunoreaction was sensitive to detect NK-1R protein in the lower level than *in situ* hybridization that detected the mRNA. I also observed moderate immunofluorescence in SN (Fig. 9); however, no additional confirmation was examined for the signal in SN. NK-1R immunoreactivity in SNr is argued against the previous reports using radioligand (Mantyh et al. 1989), *in situ* hybridization (Allen Institute Brain Atlas), and immunohistochemistry (Liu et al. 1994), although a few investigations reported NK-1R expression in SN(r) (Quirion et al. 1983; Whitty et al. 1995; Futami et al. 1998; Lessard and Pickel 2005; Lévesque et al. 2007). Since I did not examine pharmacological effects on SNr neurons, I could not further discuss the signal in SNr. In the striatum, thin neurites with puncta, which are putative axons, were also immunoreactive (Fig. 9e; Jakab and Goldman-Rakic 1996), whereas mainly somata were labeled in SN (Fig. 9e). Although a small number of observations have suggested possibility of the existence of NK-1R or substance P-binding sites in SN (Quirion et al. 1983; Whitty et al. 1995; Futami et al. 1998; Lessard and Pickel 2005; Lévesque et al. 2007), it is beyond the aim of this study to discuss on SN.

In addition, I also examined two different antibodies for each molecular marker, other than Lhx6 (Table 1). I found they provided similar images for each marker (data not shown), which suggests our present cell classification was reliable.

Although NK-1R transgenic mice were not available in this study, the use of NK-1R knock out mice might clearly resolve the discrepancy between immunofluorescence and *in situ* hybridization, which showed different NK-1R expression in GP.

For electrophysiological experiments, two points should be noted. First, I could not employ a perforated patch method, and it must cause disruption of intracellular environment which, in turn, modulate firing properties. Therefore, care should be taken for comparison the present results, e.g. spontaneous activity, with other researches. Second, fast onset and offset of response to SP receptor agonist was inconsistent with generally known behavior of metabotropic receptors, although some earlier researches also provided relatively fast effect caused by SP (Role 1984; Shen and North 1992; Lévesque et al. 2003). One possibility of discrepancy might be usage of puff stimulation using high concentration of agonist in the present research. The control experiments using ACSF puff stimulation or NK-1R antagonist supported the observed effects were caused by SM-SP, although still other possibilities could not be completely ruled out, and the intracellular mechanism should be identified in the future.

4.2. Substance P receptor agonist effects exclusively on prototypic neurons in GP

To recognize the possible role of SP in the basal ganglia, I first examined the types of GP neurons which expressed NK-1R (Fig. 13). In mice, the proportions of PV neurons range from 29 to 55%, and the extents of Lhx6 co-expression are highly variable with Lhx6 transgenic mice (Nóbrega-Pereira et al. 2010; Mastro et al. 2014; Dodson et al. 2015; Hernández et al. 2015). In the present study, which is the first study of quantitative count for Lhx6 neurons identified by immunofluorescence in wild-type mouse GP, 55% of GP neurons and 50% of PV neurons were found to co-express Lhx6. I observed slight differences on strength of Lhx6-immunefluorescence among neurons, similar to EGFP signal strength in an Lhx6-EGFP transgenic mouse line (Dodson et al. 2015). One possible reason for this discrepancy, therefore, may be the difference in the amount of Lhx6 production in GP. Another reason may be the difference in the lines of transgenic rodents and animal species. Because other data were obtained from Sprague-Dawley rats (Abdi et al. 2015) and Lhx6 transgenic mice (Nóbrega-Pereira et al. 2010; Mastro et al. 2014; Dodson et al. 2015; Hernández et al. 2015) in previous reports, further accumulation of data is necessary for wild-type and various lines of transgenic rodents. With regard to expression of PV and/or Lhx6 in prototypic neurons, again some discrepancies were observed. In our sample, 61 and 81% of prototypic neurons expressed PV and Lhx6, respectively. In previous reports, the proportion of PV expression in prototypic neurons was beyond 90% in rat (Abdi et al. 2015) and mouse (Hernández et al. 2015), whereas that of Lhx6 was 41% in mouse (Hernández et

al. 2015). Again, I could not explain these discrepancies at this time, although methodological differences (tracers, strains, species, and the way of detection of molecules: transgene vs. immunofluorescence) may affect the results. The dichotomous cell classification is emphasized by the findings that PV/NK2 homeobox 1/Lhx6-expressing prototypic neurons are comprised of major STN-innervating GP cell population and that in rats, FoxP2-expressing arkypallidal neurons do not innervate STN but rather innervate the striatum (Abdi et al. 2015). In the present study, retrograde tracing combined with immunofluorescence revealed that 67.1% of pallidosubthalamic and 25.9% of pallidostriatal neurons showed NK-1R immunoreactivity. This suggests that the NK-1R immunoreactive neurons, as a whole population, preferentially projected to STN rather than the striatum (Figs. 15, 16). It is not clear, however, whether the population of NK-1R neurons is uniformity of prototypic neurons or assembly of prototypic and arkypallidal neurons. As previously reported, dichotomous cell classification was defined by the molecular signatures and developmental fate (Nóbrega-Pereira et al. 2010; Abdi et al. 2015; Dodson et al. 2015;

Hernández et al. 2015). In the present study, in only a few NK-1R neurons, FoxP2 was detected, and the majority of pallidostriatal neurons expressing NK-1R showed Lhx6 immunoreactivity (Figs. 13, 16). Since Lhx6 neurons have been considered as prototypic neurons with striatal axon collaterals (Abdi et al., 2015), it is highly probable that the NK-1R neurons are prototypic neurons (Fig. 21).

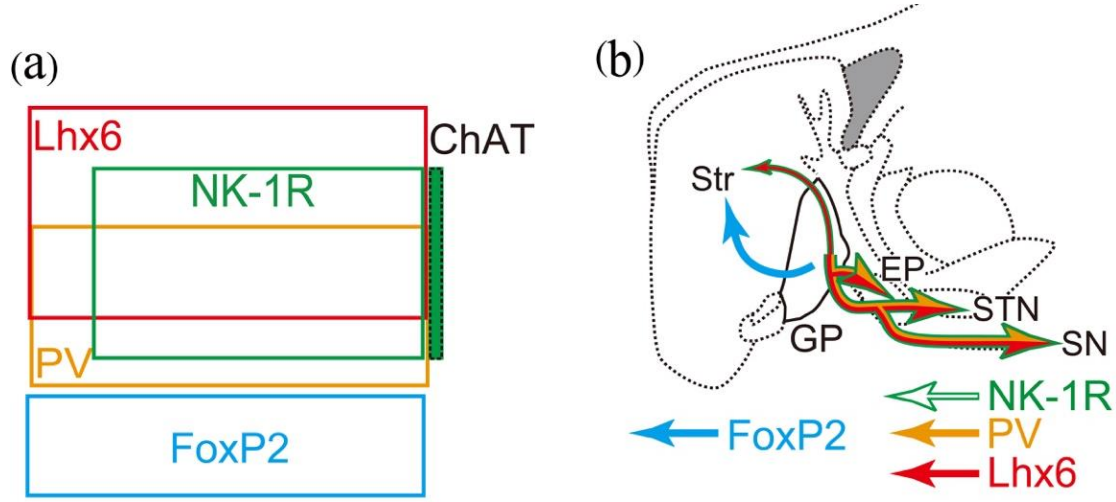

Figure 21. Immunofluorescent characteristics and projection patterns of GP neurons. **a** Schematic summary of the major neurons in the GP of mouse. *Colored* areas are scaled to show the relative population sizes of GP neurons. Note that neurokinin-1 receptor (NK-1R) neurons (*green*) express Lhx6 (*red*) and/or PV (*orange*) but not FoxP2 (*blue*). A *filled green rectangle* indicates GP representing strong NK-1R expression, which co-express choline acetyltransferase (ChAT, shown in a *dotted black line*). **b** Schematic summary of the prototypic and arkypallidal neurons. The majority of prototypic neurons express Lhx6, PV, and/or NK-1R, but not FoxP2. *Arrow size* and *line thickness* reflect relative strength of projection. *Str*, striatum; *STN*, subthalamic nucleus; *EP*, entopeduncular nucleus; *SN*, substantia nigra.

The differential co-localization rate of PV or Lhx6 immunoreactivity with NK-1R in pallidostriatal neurons (Fig. 16) suggested the nonuniform distribution and density of axon collaterals in the striatum between PV and Lhx6 neurons and possible differentiation

between Lhx6/PV and Lhx6-/PV neurons, which comprised around half of PV neuron population in the GP, respectively (Fig. 13; Fig. 14). This result is consistent with previous reports that PV neurons were restricted to prototypic neurons with few striatal collaterals rather than Lhx6 neurons in rats (Abdi et al. 2015) and mice (Hernández et al. 2015).

I revealed that SM-SP induced inward current in 21 neurons, which were resistant against glutamate and $GABA_A$ receptor antagonists, whereas 27 neurons did not respond to SM-SP (Fig. 17). The depolarizing effect of SM-SP and its voltage dependence were similar with earlier reports in the GP (Chen et al. 2009) and amygdala (Sosulina et al. 2015). Chen et al. (2009) studied the ionic mechanism of SP-induced inward current and found that the SM-SP effect was associated with increment of the membrane input resistance. They also estimated that the reversal potential was -95 mV, close to the potassium equilibrium potential. It suggested that potassium channels which usually open may close by SM-SP. Indeed, potassium channel blockers blocked the SM-SP inward current. Consistent with previous reports (Abdi et al. 2015; Hernández et al. 2015), I indicated GP neurons could be classified into at least two distinct types with regard to firing properties using the cluster analysis (Figs. 19, 20). I also revealed that CL2 and 3 contained both of SM-SP-responsive and non-responsive neurons, whereas CL1 neurons would be composed of SM-SP-non-responsive ones (Fig. 20). Considering with immunofluorescent properties and projection types (Figs. 13, 15, 16), CL1 is likely to be FoxP2-postive neurons that did not express NK-1R. On the contrary, CL2 and CL3 would be a PV/Lhx6-positive and FoxP2-negative group. In addition,

firing and immunofluorescent properties of our samples were in accordance with earlier reports (Abdi et al. 2015), and I could strongly suggest that CL1 corresponds to arkypallidal and CL2/3 to prototypic neurons. Altogether, our results insisted SM-SP affected only prototypic GP neurons, however, also contained Lhx6 neurons projecting to both the striatum and STN. SM-SP induced response would be possibly elicited via NK-1R, irrespective of the fact that NK-3R is also present in GP (Fig. 10; Furuta et al. 2004; Lévesque et al. 2006), because SM-SP and SR140333 is known as a potent and selective agonist and antagonist for NK-1R, respectively.

In the classical basal ganglia model, striatal direct pathway neurons may lead to temporary inhibition of the output nuclei, EP/SNr via the direct pathway and disinhibition of the target regions (the thalamus and cerebral cortex), allowing the occurrence of selected movements (Alexander and Crutcher 1990; Mink and Thach 1993; Houk et al. 2007). It is known that only direct pathway neurons contain SP in the striatal projection neurons. The present study, however, revealed that some prototypic neurons in the GP with distinct physiological properties were affected by SM-SP via NK-1R.

Recent study showed that the striatal axon collaterals in GP inhibit the GP neurons *in vivo* (Cazola et al, 2014). In the report, the direct and indirect pathways were selectively stimulated by the optogenetics. Laser stimulation of direct pathway neurons led to an inhibition of basal firing rate of GP neurons, which was smaller than the case of the indirect pathway neurons. Considering the electrophysiological results in the present study, the

difference in the inhibition by the direct and indirect pathway neurons may be caused by the SP, which could be co-released with GABA, by the direct pathway neurons. Further studies *in vivo* and *in vitro* will be required to clarify how the SP co-works with GABA on NK-1R expressing GP neurons. It might be a key to reveal how the striatal direct pathway neurons modulate the GP in the specific way different from indirect pathway neurons.

SP would be observed between striatal direct pathway neurons and the NK-1R neurons in the GP. This future study might contribute to clarify the basal ganglia network beyond direct/indirect pathway model.

It is suggested that the direct pathway neurons interfere with the indirect pathway via the distinct prototypic neurons and lead to disinhibition of the EP/SNr via the GP-(STN)-EP/SNr pathway and to inhibition of the thalamus and cerebral cortex. The direct pathway neurons rarely contribute to the recurrent circuit between the GP and striatum via arkypallidal neurons. Hence, EP/SNr neurons may receive not only monosynaptic but also polysynaptic input from the identical striatal direct pathway neurons. It should be noted that in comparison with fast and phasic inhibition via ionotropic $GABA_A$ receptors, metabotropic NK-1R might function on a longer time scale and in multiple ways. It is not clear when SP is released and how much SP modifies the effects of GABA. However, it could be possible that GABA and SP are contained in a single neuron, when the neuron is active, they can be released at the same time. In addition, if striatal projection neurons were an actual source of SP in the GP, both SP and GABA must be released simultaneously and then they might

interact with each other resulting in more complex effects *in vivo*. It is unclear whether pallidostriatal collaterals of prototypic neurons, which typically originated from Lhx6/PV neurons (Fig. 15; Abdi et al. 2015), function in a different way from those of arkypallidal neurons other than their distinct timing of firing (Mallet et al. 2012; Dodson et al. 2015). In the present study, I showed that not only transcription factors, but the expression of a receptor for neurochemical was also strictly distinguished between those groups. It implicates that axon terminals in the striatum of both types of GP neurons could be differentiated with regard to physiological and functional aspects.

Certainly, further researches are required to clarify functional differences between the projections of the direct and indirect pathway neurons to GP in details and their effects on the basal ganglia.

5. References

1. Abdi A, Mallet N, Mohamed FY, Sharott A, Dodson PD, Nakamura KC, Suri S, Avery SV, Larvin JT, Garas FN, Garas SN, Vinciati F, Morin S, Bezard E, Baufreton J, Magill PJ (2015) Prototypic and arkypallidal neurons in the dopamine-intact external globus pallidus. J Neurosci 35:6667–6688. doi: 10.1523/JNEUROSCI.4662-14.2015
2. Albin RL, Young AB, Penney JB (1989) The functional anatomy of basal ganglia disorders. Trends Neurosci 12:366–375. doi: 10.1016/0166-2236(89)90074-X
3. Alexander GE, Crutcher MD (1990) Functional architecture of basal ganglia circuits: neural substrates of parallel processing. Trends Neurosci. 13:266–271. doi:10.1016/0166-2236(90)90107-L
4. Aosaki T, Kawaguchi Y (1996) Actions of substance P on rat neostriatal neurons in vitro. J Neurosci 16:5141–5153.
5. Bailey CP, Maubach KA, Jones RS (2004) Neurokinin-1 receptors in the rat nucleus tractus solitarius: pre- and postsynaptic modulation of glutamate and GABA release. Neuroscience 127:467-79.
6. Bevan MD, Booth P, Eaton S, Bolam JP (1998) Selective innervation of neostriatal interneurons by a subclass of neuron in the globus pallidus of the rat. J Neurosci 18:9438–52.
7. Bevan MD, Magill PJ, Terman D, Bolam JP, Wilson CJ (2002) Move to the rhythm: Oscillations in the subthalamic nucleus-external globus pallidus network. Trends Neurosci.

25:525–531. doi:10.1016/S0166-2236(02)02235-X.

8. Blomeley C and Bracci E (2008) Substance P depolarizes striatal projection neurons and facilitates their glutamatergic inputs. J Physiol 586(8):2143-55. doi: 10.1113/jphysiol.2007.148965.

9. Cazorla M, de Carvalho FD, Chohan MO, Shegda M, Chuhma N, Rayport S, Ahmari SE, Moore H, Kellendonk C (2014) Dopamine D2 receptors regulate the anatomical and functional balance of basal ganglia circuitry. Neuron 81:153–64. doi: 10.1016/j.neuron.2013.10.041

10. Chen L, Cui Q-L, Yung WH (2009) Neurokinin-1 receptor activation in globus pallidus. Front Neurosci 3:58. doi: 10.3389/neuro.23.002.2009

11. Cooper AJ, Stanford IM (2000) Electrophysiological and morphological characteristics of three subtypes of rat globus pallidus neurone in vitro. J Physiol 527 Pt 2:291–304. doi: 10.1111/j.1469-7793.2000.t01-1-00291.x

12. Costa RM, Cohen D, Nicolelis MA. Differential corticostriatal plasticity during fast and slow motor skill learning in mice. Curr Biol. 14(13):1124-34. doi: 10.1016/j.cub.2004.06.053

13. Cui G, Jun SB, Jin X, Pham MD, Vogel SS, Lovinger DM, Costa RM. (2013) Concurrent activation of striatal direct and indirect pathways during action initiation. Nature 494:238–42. doi: 10.1038/nature11846

14. Cui QL, Yung WH, Xue Y, Chen L (2007) Substance P excites globus pallidus neurons in

vivo. Eur J Neurosci 26:1853–1861. doi: 10.1111/j.1460-9568.2007.05803.x

15. DeLong MR (1990) Primate models of movement disorders of basal ganglia origin. Trends Neurosci. 13:281–285. doi:10.1016/0166-2236(90)90110-V.

16. Dodson PD, Larvin JT, Duffell JM, Garas FN, Doig NM, Kessaris N, Duguid IC, Bogacz R, Butt SJ, Magill PJ (2015) Distinct developmental origins manifest in the specialized encoding of movement by adult neurons of the external globus pallidus. Neuron 86:501–513. doi: 10.1016/j.neuron.2015.03.007

17. Eid L, Parent A, Parent M (2016) Asynaptic feature and heterogeneous distribution of the cholinergic innervation of the globus pallidus in primates. Brain Struct Funct 221:1139–1155. doi: 10.1007/s00429-014-0960-0

18. Elde R, Schalling M, Ceccatelli S, Nakanishi S, Hökfelt T (1990) Localization of neuropeptide receptor mRNA in rat brain: Initial observations using probes for neurotensin and substance P receptors. Neurosci Lett 120:134–138. doi: 10.1016/0304-3940(90)90187-E

19. Flandin P, Kimura S, Rubenstein JL (2010) The progenitor zone of the ventral medial ganglionic eminence requires Nkx2-1 to generate most of the globus pallidus but few neocortical interneurons. J Neurosci 30:2812–2823. doi: 10.1523/JNEUROSCI.4228-09.2010

20. Fujiyama F, Nakano T, Matsuda W, Furuta T, Udagawa J, Kaneko T (2015) A single-neuron tracing study of arkypallidal and prototypic neurons in healthy rats. Brain Struct

Funct 1–8. doi: 10.1007/s00429-015-1152-2

21. Fujiyama F, Sohn J, Nakano T, Furuta T, Nakamura KC, Matsuda W, Kaneko T (2011) Exclusive and common targets of neostriatofugal projections of rat striosome neurons: a single neuron-tracing study using a viral vector. Eur J Neurosci 33:668–677. doi: 10.1111/j.1460-9568.2010.07564.x

22. Furuta T, Koyano K, Tomioka R, Yanagawa Y, Kaneko T (2004) GABAergic basal forebrain neurons that express receptor for neurokinin B and send axons to the cerebral cortex. J Comp Neurol 473:43–58. doi: 10.1002/cne.20087

23. Furuta T, Kaneko T, Deschénes M (2009) Septal neurons in barrel cortex derive their receptive field input from the lemniscal pathway. J Neurosci 29:4089–4095. doi: 10.1523/JNEUROSCI.5393-08.2009

24. Futami T, Hatanaka Y, Matsushita K, Furuya S (1998) Expression of substance P receptor in the substantia nigra. Mol Brain Res 54:183-198. doi: 10.1016/S0169-328X(97)00307-0

25. Ge SN, Ma YF, Hioki H, Wei YY, Kaneko T, Mizuno N, Gao GD, Li JL (2010) Coexpression of VGLUT1 and VGLUT2 in trigeminothalamic projection neurons in the principal sensory trigeminal nucleus of the rat. J Comp Neurol 518:3149–3168. doi: 10.1002/cne.22389

26. Gerfen CR, Engber TM, Mahan LC, Susel Z, Chase TN, Monsma FJ Jr, Sibley DR (1990) D1 and D2 dopamine receptor-regulated gene expression of striatonigral and striatopallidal neurons. Science. 250(4986):1429-32. doi: 10.1126/science.2147780

27. Gerfen CR (1991) Substance P (neurokinin-1) receptor mRNA is selectively expressed in cholinergic neurons in the striatum and basal forebrain. Brain Res 556:165–170. doi: 10.1016/0006-8993(91)90563-B

28. Gittis AH, Berke JD, Bevan MD, Chan CS, Mallet N, Morrow MM, Schmidt R (2014) New roles for the external globus pallidus in basal ganglia circuits and behavior. J Neurosci 34:15178–15183. doi: 10.1523/JNEUROSCI.3252-14.2014

29. Gomez-Gallego M, Fernandez-Villalba E, Fernandez-Barreiro A, Herrero MT (2007) Changes in the neuronal activity in the pedunculopontine nucleus in chronic MPTP-treated primates: an in situ hybridization study of cytochrome oxidase subunit I, choline acetyl transferase and substance P mRNA expression. J Neural Transm 114:319–26. doi: 10.1007/s00702-006-0547-x

30. Govindaiah G, Wang Y, Cox CL (2010) Substance P selectively modulates GABA(A) receptor-mediated synaptic transmission in striatal cholinergic interneurons. Neuropharmacology 58:413-22 doi: 10.1016/j.neuropharm.2009.09.011

31. Graybiel AM (1990) Neurotransmitters and neuromodulators in the basal ganglia. Trends Neurosci. 13:244–254.doi:10.1016/0166-2236(90)90104-I

32. Hama H, Hioki H, Namiki K, Hoshida T, Kurokawa H, Ishidate F, Kaneko T, Akagi T, Saito T, Saido T, Miyawaki A (2015) ScaleS: an optical clearing palette for biological imaging. Nat Neurosci 18:1518–29. doi: 10.1038/nn.4107

33. Hernández VM, Hegeman DJ, Cui Q, Kelver DA, Fiske MP, Glajch KE, Pitt JE, Huang

TY, Justice NJ, Chan CS (2015) Parvalbumin+ neurons and Npas1+ neurons are distinct neuron classes in the mouse external globus pallidus. J Neurosci 35:11830–11847. doi: 10.1523/JNEUROSCI.4672-14.2015

34. Hikosaka O, Takikawa Y, Kawagoe R (2000) Role of the basal ganglia in the control of purposive saccadic eye movements. Physiol Rev. 80(3):953-78.

35. Hioki H, Nakamura H, Ma YF, Konno M, Hayakawa T, Nakamura KC, Fujiyama F, Kaneko T (2010) Vesicular glutamate transporter 3-expressing nonserotonergic projection neurons constitute a subregion in the rat midbrain raphe nuclei. J Comp Neurol 518:668–686. doi: 10.1002/cne.22237

36. Hong JS and Costa E (1978) Participation of substance P in the action of haloperidol. Psychopharmacol Bull. 14(4):23-4.

37. Hong JS, Yang H, Fratta W, Costa E (1978) Rat striatal methionine-enkephalin content after chronic treatment with cataleptogenic and noncataleptogenic antischizophrenic drugs. J Pharmacol Exp Ther. 205(1):141-7.

38. Hoover BR, Marshall JF (2002) Further characterization of preproenkephalin mRNA-containing cells in the rodent globus pallidus. Neuroscience 111:111–125. doi: 10.1016/S0306-4522(01)00565-6

39. Houk JC, Bastianen C, Fansler D, Fishbach A, Fraser D, Reber PJ, Roy SA, Simo LS (2007) Action selection and refinement in subcortical loops through basal ganglia and cerebellum. Philos Trans R Soc Lond B Biol Sci 362:1573–1583. doi:

10.1098/rstb.2007.2063

40. Isomura Y, Takekawa T, Harukuni R, Handa T, Aizawa H, Takada M, Fukai T (2013) Reward-modulated motor information in identified striatum neurons. J Neurosci 33:10209–20. doi: 10.1523/JNEUROSCI.0381-13.2013

41. Jakab RL, Goldman-Rakic P (1996) Presynaptic and postsynaptic subcellular localization of substance P receptor immunoreactivity in the neostriatum of the rat and rhesus monkey (Macaca mulatta). J Comp Neurol 369(1):125-136. doi: 10.1002/(SICI)1096-9861(19960520)369:1<125::AID-CNE9>3.0.CO;2-5

42. Jin X, Tecuapetla F, Costa RM (2014) Basal ganglia subcircuits distinctively encode the parsing and concatenation of action sequences. Basal ganglia subcircuits distinctively encode the parsing and concatenation of action sequences. Nat Neurosci. (3):423-30. doi: 10.1038/nn.3632.

43. Kameda H, Hioki H, Tanaka YH, Tanaka T, Sohn J, Sonomura T, Furuta T, Fujiyama F, Kaneko T (2012) Parvalbumin-producing cortical interneurons receive inhibitory inputs on proximal portions and cortical excitatory inputs on distal dendrites. Eur J Neurosci 35:838–854. doi: 10.1111/j.1460-9568.2012.08027.x

44. Kawaguchi Y, Wilson CJ, Emson PC (1990) Projection subtypes of rat neostriatal matrix cells revealed by intracellular injection of biocytin. J Neurosci 10:3421–38. http://www.jneurosci.org/content/10/10/3421

45. Kertes E, László K, Berta B, Lénárd L (2009) Positive reinforcing effects of substance P

in the rat central nucleus of amygdala. Behav Brain Res. 205(1):307-10. doi: 10.1016/j.bbr.2009.06.028.

46. Kita H (2007) Globus pallidus external segment. Prog. Brain Res. 160:111–133.

47. Kita H, Kitai ST (1994) The morphology of globus pallidus projection neurons in the rat: an intracellular staining study. Brain Res. 636:308–319. doi: 10.1016/0006-8993(94)91030-8

48. Kombian SB, Ananthalakshmi KV, Parvathy SS, Matowe WC (2003) Substance P depresses excitatory synaptic transmission in the nucleus accumbens through dopaminergic and purinergic mechanisms. J Neurophysiol 89:728-37. doi: 10.1152/jn.00854.2002

49. Kuramoto E, Furuta T, Nakamura KC, Unzai T, Hioki H, Kaneko T (2009) Two types of thalamocortical projections from the motor thalamic nuclei of the rat: A single neuron-tracing study using viral vectors. Cereb Cortex 19:2065–2077. doi: 10.1093/cercor/bhn231

50. Lee T, Kaneko T, Taki K, Mizuno N (1997) Preprodynorphin-, preproenkephalin-, and preprotachykinin-expressing neurons in the rat neostriatum: An analysis by immunocytochemistry and retrograde tracing. J Comp Neurol 386:229–244. doi: 10.1002/(SICI)1096-9861(19970922)386:2<229::AID-CNE5>3.0.CO;2-3

51. Lessard A, Pickel VM (2005) Subcellular distibution of and plasticity of neurokinin-1 receptors in the rat substantia nigra and ventral tegmental area. Neurosci 135: 1309-1323.

doi:10.1016/j.neuroscience.2005.07.025

52. Lévesque M, Wallman MJ, Parent R, Sík A, Parent A (2007) Neurokinin-1 and neurokinin-3 receptors in primate substantia nigra. Neurosci Res 57:362-371. doi: 10.1016/j.neures.2006.11.002

53. Lévesque M, Bédard A, Cossette M, Parent A (2003) Novel aspects of the chemical anatomy of the striatum and its efferents projections. J Chem Neuroanat 26:271–281. doi: 10.1016/j.jchemneu.2003.07.001

54. Lévesque M, Parent A (2005) The striatofugal fiber system in primates: a reevaluation of its organization based on single-axon tracing studies. Proc Natl Acad Sci U S A 102:11888–93. doi: 10.1073/pnas.0502710102

55. Lévesque M, Parent R, Parent A (2006) Cellular and subcellular localization of neurokinin-1 and neurokinin-3 receptors in primate globus pallidus. Eur J Neurosci 23:2760–2772. doi: 10.1111/j.1460-9568.2006.04800.x

56. Liu H, Brown JL, Jasmin L, Maggio JE, Vigna SR, Mantyh PW, Basbaum AI (1994) Synaptic relationship between substance P and the substance P receptor: Light and electron microscopic characterization of the mismatch between neuropeptides and their receptors. Proc Natl Acad Sci USA 91: 1009-1013.

57. Ma Y, Hioki H, Konno M, Pan S, Nakamura H, Nakamura KC, Furuta T, Li JL, Kaneko T (2011) Expression of gap junction protein connexin36 in multiple subtypes of gabaergic neurons in adult rat somatosensory cortex. Cereb Cortex 21:2639–2649. doi:

10.1093/cercor/bhr051

58. Mallet N, Micklem BR, Henny P, Brown MT, Williams C, Bolam JP, Nakamura KC, Magill PJ (2012) Dichotomous organization of the external globus pallidus. Neuron 74:1075–1086. doi: 10.1016/j.neuron.2012.04.027

59. Mallet N, Schmidt R, Leventhal D, Chen F, Amer N, Boraud T, Berke JD (2016) Arkypallidal cells send a stop signal to striatum. Neuron 89:308–316. doi: 10.1016/j.neuron.2015.12.017

60. Mantyh PW, Hunt SP, Maggio JE (1984) Substance P receptors: Localization by light microscopic autoradiography in rat brain using [3H]SP as the radioligand. Brain Res 307:147–165. doi: 10.1016/0006-8993(84)90470-0

61. Mastro KJ, Bouchard RS, Holt HK, Gittis AH (2014) Transgenic mouse lines subdivide external segment of the globus pallidus (GPe) neurons and reveal distinct GPe output pathways. J Neurosci 34:2087–2099. doi: 10.1523/JNEUROSCI.4646-13.2014

62. Maubach KA, Martin K, Smith DW, Hewson L, Frankshun RA, Harrison T, Seabrook GR (2001) Substance P stimulates inhibitory synaptic transmission in the guinea pig basolateral amygdala *in vitro.* Neuropharmacology 40:806-17. doi: 10.1016/S0028-3908(00)00209-4

63. Mileusnic D, Magnuson DJ, Hejna MJ, Lorens JB, Lorens SA, Lee JM (1999) Age and species-dependent differences in the neurokinin B system in rat and human brain. Neurobiol. Aging 20:19–35. doi:10.1016/S0197-4580(99)00019-6.

64. Mink JW (1996) The basal ganglia: Focused selection and inhibition of competing motor programs. Prog. Neurobiol. 50:381–425. doi:10.1016/S0301-0082(96)00042-1.

65. Mink JW, Thach WT (1993) Basal ganglia intrinsic circuits and their role in behavior. Curr Opin Neurobiol 3:950–957. doi: 10.1016/0959-4388(93)90167-W

66. Mizutani K, Takahashi S, Okamoto S, Karube F, Fujiyama F (2017) Substance P effects exclusively on prototypic neurons in mouse globus pallidus Brain Struct Funct Fast online doi: 10.1007/s00429-017-1453-8

67. Mounir S, Parent A (2002) The expression of neurokinin-1 receptor at striatal and pallidal levels in normal human brain. Neurosci Res 44:71–81. doi: 10.1016/S0168-0102(02)00087-1

68. Nakaya Y, Kaneko T, Shigemoto R, Nakanishi S, Mizuno N (1994) Immunohistochemical localization of substance P receptor in the central nervous system of the adult rat. J Comp Neurol 347:249–74. doi: 10.1002/cne.903470208

69. Nambu A, Llinás R (1994) Electrophysiology of globus pallidus neurons in vitro. J Neurophysiol 72:1127–1139.

70. Nambu A, Llinás R (1997) Morphology of globus pallidus neurons: Its correlation with electrophysiology in guinea pig brain slices. J Comp Neurol 377:85–94. doi: 10.1002/(SICI)1096-9861(19970106)377:1<85::AID-CNE8>3.0.CO;2-F

71. Nambu A, Tokuno H, Takada M (2002) Functional significance of the cortico-subthalamo-pallidal "hyperdirect" pathway. Neurosci. Res. 43:111–117.

doi:10.1016/S0168-0102(02)00027-5

72. Nóbrega-Pereira S, Gelman D, Bartolini G, Pla R, Pierani A, Marín O (2010) Origin and molecular specification of globus pallidus neurons. J Neurosci 30:2824–2834. doi: 10.1523/JNEUROSCI.4023-09.2010

73. Obeso J, Rodríguez-Oroz MC, Benitez-Temino B, Blesa FJ, Guridi J, Marin C, Rodriguez M (2008) Functional organization of the basal ganglia: therapeutic implications for Parkinson's disease. Mov Disord 23 Suppl 3:S548-59. doi: 10.1002/mds.22062

74. Parent A, De Bellefeuille L (1983) The pallidointralaminar and pallidonigral projections in primate as studied by retrograde double-labeling method. Brain Res 278:11–27. doi: 10.1016/0006-8993(83)90222-6

75. Paxinos G, Franklin KB (2013) The mouse brain in stereotaxic coordinates. 4th Ed.Elsevier, Amsterdam.

76. Quirion R, Shults CW, Moody TW, Pert CB, Chase TN, O'Donohue TL (1983) Autoradiographic distribution of substance P receptors in rat central nervous system. Nature 303:714-716. doi:10.1038/303714a0

77. Role LW (1984) Substance P modulation of acetylcholine-induced currents in embryonic chicken sympathetic and ciliary ganglion neurons. Proc Natl Acad Sci U S A 81:2924–8.

78. Sadek AR, Magill PJ, Bolam JP (2007) A single-cell analysis of intrinsic connectivity in the rat globus pallidus. J Neurosci 27:6352–62. doi: 10.1523/JNEUROSCI.0953-07.2007

79. Sato F, Lavallée P, Lévesque M, Parent A (2000) Single-axon tracing study of neurons of

the external segment of the globus pallidus in primate. J Comp Neurol 417:17–31. doi: 10.1002/(SICI)1096-9861(20000131)417:1<17::AID-CNE2>3.0.CO;2-I

80. Saunders A, Oldenburg IA, Berezovskii VK, Johnson CA, Kingery ND, Elliott HL, Xie T, Gerfen CR, Sabatini BL (2014) A direct GABAergic output from the basal ganglia to frontal cortex. Nature 521:85-9. DOI: 10.1038/nature14179

81. Shen KZ, North RA (1992) Substance P opens cation channels and closes potassium channels in rat locus coeruleus neurons. Neuroscience 50:345–353. doi: 10.1016/0306-4522(92)90428-5

82. Shughrue PJ, Lane M V, Merchenthaler I (1996) In situ hybridization analysis of the distribution of neurokinin-3 mRNA in the rat central nervous system. J Comp Neurol 372:395–414.doi: 10.1002/(SICI)1096-9861(19960826)372:3<395::AID-CNE5>3.0.CO;2-Y

83. Smith Y, Bevan MD, Shink E, Bolam JP (1998) Microcircuitry of the direct and indirect pathways of the basal ganglia. Neuroscience 86:353–387. doi: 10.1016/S0306-4522(98)00004-9

84. Smith Y, Bolam JP (1989) Neurons of the substantia nigra reticulata receive a dense GABA-containing input from the globus pallidus in the rat. Brain Res 493:160–167. doi: 10.1016/0006-8993(89)91011-1

85. Sosulina L, Strippel C, Romo-Parra H, Walter AL, Kanyshkova T, Sartori SB, Lange MD, Singewald N, Pape HC (2015) Substance P excites GABAergic neurons in the mouse

central amygdala through neurokinin 1 receptor activation. J Neurophysiol 2:jn. doi: 10.1152/jn.00883.2014

86. Stephenson-Jones M, Samuelsson E, Ericsson J, Robertson B, Grillner S (2011) Evolutionary conservation of the basal ganglia as a common vertebrate mechanism for action selection. Curr Biol 21:1081–1091. doi: 10.1016/j.cub.2011.05.001

87. Vincent SR, Satoh K, Armstrong DM, Fibiger HC (1983) Substance P in the ascending cholinergic reticular system. Nature 306:688–691. doi:10.1038/306688a0

88. Ward JH (1963) Hierarchical grouping to optimize an objective function. J. Am. Stat. Assoc. 58:236–244.

89. Wichmann T, Delong MR (1996) Functional and pathophysiological models of the basal ganglia. Curr. Opin. Neurobiol. 6:751–758. doi: 10.1016/S0959-4388(96)80024-9

90. Whitty CJ, Walker PD, Goebel DJ, Poosch MS, Bannon MJ (1995) Quantitation, cellular localization and regulation of neurokinin receptor gene expression within the rat substantia nigra. Neurosci 64: 419-425. doi:10.1016/0306-4522(94)00373-D